Doctorate Dissertation

博士論文

Characterization of peribiliary gland-constituting cells based on expression of Trop2 in mouse biliary tract

(Trop2 の発現を指標としたマウス胆管周囲付属腺細胞の性状解析)

A Dissertation Submitted for Degree of Doctor of Philosophy

December 2017

平成 **29** 年 **12** 月　博士（理学）申請

Department of Biological Sciences, Graduate School of Science,

The University of Tokyo

東京大学大学院理学系研究科生物科学専攻

Satoshi Matsui

松井 理司

Table of contents

Abbreviations

2-AAF: 2-Acetylaminofluorene

3'-Me-DAB: 3'-methyl-4dimethyl aminoazobenzene

Ae2: Anion exchanger protein 2

AGM: Aorta-gonad mesonephros

Afp: Alpha fetoprotein

Alb: Albumin

ALDH: Aldehyde dehydrogenase

Amy2a5: Amylase 2a5

APAP: Acetaminophen

APC: Allophycocyanin

Ascl2: Achaete-scute family bHLH transcription factor 2

BABB: Benzyl alcohol/benzyl benzoate

BD: Bile duct

BDL: Bile duct ligation

BEC: Biliary epithelial cell

BSA: Bovine serum albumin

BTSC: Biliary tree stem/progenitor cell

BrdU: 5-bromo-2´-deoxyuridine

CBD: Common bile duct

CCl_4: Carbon tetrachloride

CD: Cystic duct

CDE: Choline-deficient, ethionine-supplemented

Cftr: Cystic fibrosis transmembrane conductance regulator

CFP: Cyan fluorescent protein

CHD: Common hepatic duct

ChgA: Chromogranin A

CK: Cytokeratin

CV: Central vein

Cy3: Cyanine dye 3

DAG: Diacylglycerol

Dclk1: Doublecortin-like kinase 1

DDC: 3,5-diethoxycarbonyl-1,4-dihydrocollidine

DEN: Diethylnitrosamine

Dipin: 1 ,4-bis [N, N'-di (ethylene)-phosphamide] pi-perazine

Dlk1: Delta like non-canonical Notch ligand 1

DMEM: Dulbecco's modified Eagle's medium

Dner: Delta and Notch-like epidermal growth factor-related receptor

E8.5: Embryonic day 8.5

EGF-L: Epidermal growth factor-like domain

EGF: Epidermal growth factor

EHBD: Extrahepatic bile duct

ERK: Extracellular signal-regulated kinase

ES cell: Embryonic stem cell

EpCAM: Epithelial cell adhesion molecule

fabp10a: Fatty acid binding protein 10a

FACS: Fluorescence activated cell sorting

FBS: Fetal bovine serum

FCM: Flow cytometric

FcR: Fc receptor

FITC: Fluorescein isothiocyanate

FGF10: Fibroblast growth factor 10

Foxl1: Forkhead box L 1

FSC: Forward scatter

GB: Gallbladder

GGT: γ-glutamyltranspeptidase

GP2: Glycoprotein 2

HA: Hepatic artery

HEPES: 4-(2-hydroxyethyl)-1-piperazineethanesulfonic acid

Hhex: Hematopoietically expressed homeobox

Hes1: Hairy and enhancer of split 1

HGF: Hepatocyte growth factor

HNF1β: Hepatocyte nuclear factor 1 beta

IBEC: Intrahepatic biliary epithelial cell

IHBD: Intrahepatic bile duct

IL33: Interleukin 33

IP3: Inositol trisphosphate

iPS cell: Induced pluripotent stem cell

ITGA6: Integrin alpha 6

ITS-X: Insulin transferrin selenium ethanolamine solution

Kras: Kirsten rat sarcoma viral oncogene homolog

KO: Knock-out

LBEC: Lumen-forming biliary epithelial cell

Lgr5: Leucine rich repeat containing G protein-coupled receptor 5

LPC: Liver stem/progenitor cell

MAPK: Mitogen-activated protein kinase

MCDE: Methionine choline-deficient diet supplemented with ethionine

MDA: Methylene dianiline

Mdm2: Mdm 2, proto-oncogene

Mdr1: Multidrug-resistance protein1

MIC1-1C3: Macrophage inhibitory cytokine 1-1C3

Muc6: Mucin 6, gastric

Nanog: Nanog, homeobox

Ngn3: Neurogenin 3

NPC: Hepatic non-parenchymal cells

NTR: Nitroreductase

Oct4: Octamer-binding transcription factor 4

Olfm4: Olfactomedin 4

Opn: Osteopontin

PBEC: PBG-constituting biliary epithelial cell

PBG: Peribiliarygland

PBS: Phosphate-buffered saline

Pdx1: Pancreatic and duodenal homeobox 1

PFA: Paraformaldehyde

PHx: Partial hepatectomy

PI: Propidium iodide

PIP_2: Phosphatidylinositol 4,5- bisphosphate

PKC: Protein kinase C

Pnlip: Pancreatic lipase

PV: Portal vein

RT: Room temperature

Sca-1: Stem cell antigen-1

SeeDB: See deep brain

Ser: Serine

Sox: Sex determining region Y-box

SP: Signal peptide

SSC: Side scatter

Sst: Somatostatin

STZ: Streptozotocin

TA cell: Transit amplifying cell

Tacstd: Tumor associated calcium signal transducer

TE: Tris-EDTA

TGFβR2: Transforming growth factor beta receptor 2

Thy1: Thymus cell antigen 1, theta

Trop2: Trophoblast cell surface protein 2

TY: Thyroglobulin type-1 repeat domain

Abstract

The bile duct, a tubular epithelial tissue, plays an important role in the drainage of bile from the liver into the small intestine. Based on histology and embryology, the bile duct is classified into the intrahepatic bile duct (IHBD) and the extrahepatic bile duct (EHBD). While IHBD forms an intricate tree-like network in the liver parenchyma, EHBD forms luminal structure that links IHBD to the duodenum. EHBD has many accessory glands, namely “peribiliary glands (PBGs)”. PBG is composed of heterogeneous cell populations such as mucus and pancreatic enzyme-producing epithelial cells, while it is known to constitute niches for multi-potential stem/progenitor cells, called “biliary tree stem/progenitor cells (BTSCs)”, in human EHBD. BTSC shows a similar gene expression profile to liver stem/progenitor cell (LPC) and pancreatic progenitor cell, having a potential for differentiating into hepatocytes, mature biliary epithelial cells (BECs) and pancreatic islets. However, there is no applicable method to isolate PBG-constituting cells from the EHBD. Therefore, the role and nature of PBGs in the mouse EHBD remains unclear. The objective of this study is to establish the method for isolating and characterizing PBG-constituting cells in the mouse EHBD.

In the present study, I found that trophoblast cell surface protein 2 (Trop2) was expressed in the luminal epithelium of mouse EHBD exclusively, but not in the PBG. Based on the differential expression profile of Trop2, the lumen-forming biliary epithelial cells (LBECs) and PBG-constituting biliary

epithelial cells (PBECs) were isolated for further characterization by gene expression analysis, immunostaining, and assays of colony and organoid formation.

Gene expression profiling revealed that the isolated mouse PBECs expressed several genes characteristic of human PBGs, fetal pancreatic progenitor and intestinal tuft cells. In the colony formation assay, PBECs showed significantly higher colony formation capacity than LBECs. The expanded PBECs showed up-regulation of Trop2 expression and down-regulation of human PBG-related genes in the 2D culture condition. In the 3D organoid formation assay, PBECs gave rise to a cysts structure with epithelial polarity, showing the gene expression patterns similar to LBECs.

Finally, I examined the expression pattern of Trop2 during EHBD regeneration after bile duct ligation (BDL), a severe cholestasis model. After BDL, the luminal epithelium was severely injured and damaged LBECs were peeled off from the lumen. On the other hand, PBECs proliferated and re-expressed Trop2 in PBGs upon EHBD injury. Next, I compared the colony formation capacity between $Trop2^{+}$ and $Trop2^{-}$ BECs after BDL and showed that the colony formation capacity of $Trop2^{+}$ BECs was dramatically increased after EHBD injury. Taking these *in vitro* and *in vivo* data together, PBGs contain progenitor-like cells with high capacity for proliferation, which supply new LBECs during biliary regeneration. Thus, Trop2 is a useful marker to investigate the pathophysiological roles and characteristics of PBGs in biliary diseases.

Introductions

Liver function and architecture

The liver is the largest organ in the body and plays essential roles for homeostasis (Burt et al., 2012). Functions of the liver drastically change with developmental stage. In the embryonic stage, the liver functions as the major hematopoietic organ that supports proliferation and differentiation of hematopoietic stem cells (HSCs) originated from the aorta-gonad mesonephros (AGM) region (Orkin et al., 2008).

As shown in Figure 1, the liver is composed of the hepatic lobules, a hexagonal structure around the central vein (CV) (Burt et al., 2012). The portal triad, consisting of the intrahepatic bile duct (IHBD), the portal vein (PV) and the hepatic artery (HA), is located in outer corners of the liver lobule (Figure 1) (Burt et al., 2012).

The liver contains various types of cells (Figure 1). Hepatocytes account for 80% of the liver mass and play a major role in liver functions. The other cells are called hepatic non-parenchymal cells (NPCs). Among them, liver sinusoidal endothelial cells (LSECs) are liver-specific endothelial cells, which form intricate vascular networks in the liver parenchyma and exchange circulating nutrients and metabolites produced by hepatocytes (Poisson et al., 2017). Kupffer cells are liver resident macrophages, residing in the lumen of the liver sinusoid, and contribute to the host defense, immunological tolerance and liver regeneration (Bilzer et al., 2006). Hepatic stellate cells are located at “space of Disse”, the

interspace between hepatocytes and liver sinusoids and involve in storage of vitamin A, inflammation and fibrosis (Tsuchida et al., 2017). Bile production is one of the important liver functions. Bile produced by hepatocytes is transported into IHBD through the bile canaliculi, a capillary structure surrounded by the apical membrane of neighboring hepatocytes (Boyer. 2013). The bile canaliculi connect with IHBDs via junctional structures, the “canal of Hering” (Saxena et al., 2004).

Biliary system

The bile duct is a single layered tubular epithelial tissue, composed of the mature biliary epithelial cells (BECs). Bile ducts play an important role for transporting bile into the duodenum. Moreover, bile ducts control fluidity of bile by ion transporters and act as an epithelial barrier to prevent leakage of toxic bile (Boyer. 2013).

Based on histology and embryology, bile ducts are classified into the IHBD and the extrahepatic bile duct (EHBD) (Figure 2A). IHBD forms a hierarchical tree-like network running along PVs (Marzioni et al., 2002; Kaneko et al., 2015) (Figure 2B). IHBD is responsive to hepatic damage and liver injury induces remodeling of its structure (Kaneko et al., 2015).

On the other hand, EHBDs are composed of the common hepatic duct (CHD), cystic duct (CD), common bile duct (CBD) and gallbladder (GB). In contrast to the intricately branching structure of IHBD, EHBD, except GB,

contains many accessory glands, namely the peribiliary glands (PBGs) in a fibromuscular layer of EHBD (Ishida et al., 1989; Nakanuma et al., 1994; Nakanuma et al., 1997) (Figure 2B-e). PBGs consist of heterogeneous cellular populations including the cells that produce mucus and pancreatic enzymes (Terada et al., 1993; Dipaola et al., 2013).

Development of IHBD and EHBD

Although both IHBD and EHBD form the flow channel of bile, these tissues are derived from distinct origins (Zong et al., 2011). IHBD originates from hepatoblast, a common progenitor cell with the hepatocyte (Figure 3). By contrast, EHBD is derived from a common primordium to the ventral pancreas (Spence et al., 2009). As shown in Figure 3, several transcriptional factors are known to be involved in the cell fate determination. Divergence of the hepatic fate (hematopoietically expressed homeobox $[Hhex]^{+}$, sex determining region Y-box 17 $[Sox17]^{-}$ pancreatic duodenal homeobox 1 $[Pdx1]^{-}$) or the pancreatobiliary fate ($Hhex^{-}$ $Pdx1^{+}$ $Sox17^{+}$) occurs at E8.5 (Bort et al., 2006; Spence et al., 2009; Zong et al., 2011). The pancreatobiliary primordium divides into the $Sox17^{+}$ biliary primordium and the $Pdx1^{+}$ pancreatic primordium at E10.5 (Spence et al., 2009). Sox17 is required for determination of the borderline between the extrahepatic biliary and the pancreatic development (Spence et al., 2009). The lack in Sox17 leads to hypoplasia of the gallbladder and the ectopic pancreatic tissue formation in EHBD (Spence et al., 2009). On the other hand,

the lack of Pdx1 leads to the loss of PBGs and mucus-producing cells in CBD (Fukuda et al., 2006). Moreover, the knock-out (KO) mouse devoid of hairy and enhancer of split 1 (Hes1), a Notch signaling-related gene, exhibits hypoplasia of the extrahepatic biliary system by the fate conversion into the pancreatic tissue (Sumazaki et al., 2004).

Tissue stem/progenitor cell

Stem cell is generally defined as an undifferentiated cell, which maintains itself by self-renewal and has a potential to differentiate into multiple types of functional progenies (Gilbert. 2012) (Figure 4). Asymmetric cell division allows stem cells to generate two distinct daughter cells, a multi-potent stem cell and a lineage committed progenitor cell (Knoblich. 2008).

Many organs contain an tissue specific stem cell or progenitor cell. Unlike the embryonic stem cells (ESCs) and the induced pluripotent stem cells (iPSCs), which are able to differentiate into all cell types, except trophoblasts, the differentiation potential of tissue stem/progenitor cells is limited (Barker et al., 2010). Upon loss of mature cells by tissue injury or life cycle, tissue stem/progenitor cells are activated to supply functional progenies (Barker et al., 2010). The undifferentiated state of the tissue stem/progenitor cells is regulated by an interaction with their microenvironment, so-called the stem cell niche (Morrison et al., 2008). To elucidate the role and nature of tissue stem/progenitor cells, large efforts have been made to isolate tissue stem/progenitor cells by

fluorescence activated cell sorting (FACS) and evaluate its potential by *in vitro* differentiation assays and cell transplantation. Recently, the genetic lineage tracing is actively carried out to elucidate the fate of stem/progenitor cells *in vivo* (Kretzschmar et al., 2012).

Liver stem/progenitor cell (LPC)

It is well known that the liver has remarkably regenerative capacity. When the liver is acutely injured by several causes such as chemicals, virus infection or metabolic disorders, liver regeneration is mainly achieved by the proliferation of remaining hepatocytes. Under chronic or severe liver injury, however, the “liver stem/progenitor cell (LPC)” have been postulated to contribute to liver regeneration by differentiating into functional hepatocytes and BECs (Figure 5) (Miyajima et al., 2014). The activated LPCs extend toward the damaged area together with the IHBD, forming luminal structures (Figure 5). This structural remodeling is known as “ductular reaction”. The LPCs are postulated to exist in the canal of Hering, a junction point between IHBD and hepatocyte (Saxena et al., 2004). The concept of the LPC was originally proposed in rat liver injury models accompanying severe hepatocyte failure and carcinogenesis (Farber. 1956). The prototypic LPC was called “oval cell”, which is named after its nuclear shape. Although the nature of the LPCs have been well-documented in many studies using rodent and fish liver injury models, LPCs are also observed in patients with hepatitis, including both acute and chronic, and fatty liver diseases

(Table 1).

LPCs have been conventionally identified based on marker expression. Previously, many markers have been reported to characterize LPCs (Table 2). However, most of those markers are not specific to LPCs because they are expressed in mature BECs as well. Of note, our research team has previously demonstrated that trophoblast antigen 2 (Trop2) is exclusively expressed in activated LPCs of injured liver, but not in mature BECs of normal liver (Okabe et al., 2009).

Biliary tree stem/progenitor cell (BTSC)

Recently it has been reported that human EHBD contains multipotent tissue stem/progenitor cells. This multipotent tissue stem/progenitor cell is named “biliary tree stem/progenitor cells (BTSCs)” (Cardinal et al., 2011). BTSCs were identified by the selective culture based on resistance for cytotoxicity (Cardinal et al., 2011). Human BTSCs show a gene expression profile similar to several stem/progenitor cells: definitive endoderm marker Sox17, LPC markers such as epithelial cell adhesion molecule [EpCAM] and sex determining region Y-box 9 [SOX9]), pancreatic progenitor cell (PDX1), ESC markers (octamer-binding transcription factor 4 [OCT4], sex determining region Y-box 2 [SOX2] and nanog, homeobox [NANOG]), and intestinal stem/progenitor cell (e.g. leucine rich repeat containing G protein coupled receptor 5 [LGR5]) (Cardinal et al., 2011; Carpino et al., 2012; Cardinale et al., 2012; Lanzoni et al., 2016). Human BTSCs

have a potential for differentiating into hepatocytes, mature BECs and pancreatic islets *in vitro* condition (Figure 6). Therefore, BTSCs are considered to be similar to the posterior foregut endodermal progenitor (Cardinale et al., 2012; Lanzoni et al., 2016). By taking advantage of human BTSC markers for immunohistochemistry, their restricted expression profile in the PBGs has demonstrated that BTSCs are localized in the bottom of the PBGs (Carpino et al., 2012; Lanzoni et al., 2016) (Figure 6). By contrast, the nature and location of the mouse BTSCs are poorly understood because Pdx1 and Sox17 are expressed throughout EHBD (Fukuda et al., 2006; Dipaola et al., 2013).

PBG has been suggested to contribute to biliary regeneration, i.e. regeneration of EHBD is achieved by the proliferation of PBGs (Cohen et al., 1964). Consistently, the proliferation of PBGs has been reported in patients with hepatolithiasis, cholangitis and type2 diabetes and rodent biliary and pancreatic injury models (Table 3). Recently, it has been reported that interleukin 33 (IL33) induces the proliferation of PBGs and luminal epithelia of EHBD in the biliary atresia model and severe epithelial cell injury models (Li et al., 2014; Nakagawa et al., 2017). In addition, up-regulation of LPC markers and a pancreatic endocrine progenitor cell marker, such as neurogenin 3 (Ngn3) was observed in patients with cholangitis, ischemic type biliary lesions and diabetes, and in rodent biliary injury and diabetes models (Irie et al., 2007; Sutton et al., 2012; Carpino et al., 2016). These results suggested the implication of PBGs in biliary or pancreatic regeneration. However, it is still unclear whether the proliferating

PBGs act as a tissue stem/progenitor cell for regeneration.

Trophoblast antigen 2 (Trop2)

Trop2, also known as tumor-associated calcium signal transducer 2 (Tacstd2), is a cell-surface glycoprotein, which was identified in the trophoblast and human carcinomas (Lipinski et al., 1981; Fornaro et al., 1995). Trop2 contains a signal peptide (SP), the epidermal growth factor-like domain (EGF-L) and the thyroglobulin type-1 repeat domain (TY) in its extracellular domain (Linnenbach et al., 1989; Linnenbach et al., 1993; Lin et al., 2012) (Figure 7). Moreover, an intracellular serine residue (S303) of Trop2 is phosphorylated by protein kinase C (PKC) and interacts with phosphatidylinositol 4,5-bisphosphate (PIP_2) (Basu et al., 1995; El Sewedy et al., 1998).

During development, Trop2 is expressed in epidermis, kidney, lung and gastrointestinal tracts, including stomach and small intestine (Tsukahara et al., 2011; Mustata et al., 2013; Fernandez Vallone et al., 2016). As developmental stage progresses, Trop2 expression is gradually decreased and restricted in specific organs (El Sewedy et al., 1998; Goldstein et al., 2008; Nakatsukasa et al., 2010; Lin et al., 2012; Sun et al., 2014). On the other hand, it has been reported that re-expression of Trop2 occurs in the injured liver, air way and stomach (Okabe et al., 2009; Fernandez Vallone et al., 2016; Liu et al., 2016). Moreover, Trop2 is also proposed as a prognostic marker and therapeutic target for various types of tumors (Fornaro et al., 1995; Ohmachi et al., 2006; Fong et

al., 2008a; Fong et al., 2008b; Mühlmann et al., 2009; Lin et al., 2012; Lin et al., 2014).

Trop2 is involved in many kinds of intracellular signals, including β-catenin, mitogen-activated protein kinase/extracellular signal-regulated kinase (MAPK/ERK) and inositol trisphosphate-diacylglycerol (IP3-DAG) pathways, and regulates cell proliferation and apoptotic cell death (Stoyanova et al., 2012; Cubas et al., 2010; Liu et al., 2013; Ripani et al., 1998; El Sewedy et al., 1998). Trop2 also regulates cell-cell adhesion via interacting with claudin-1 and -7 (Nakatsukasa et al., 2010). On the other hand, Trop2 exhibits high degree of protein sequence homology with EpCAM. Therefore, Trop2 shares its molecular functions and binding partners with EpCAM (Maetzel et al., 2009; Wu et al., 2013; McDougall et al., 2015).

Aim of this study

As mentioned above, human BTSCs have been identified by a long-term selective culture of dissociated EHBD-constituting cells, which include various types of cells as well as PBG-constituting cells. Therefore, there is no direct evidence that the PBG is the origin of BTSCs. Even if PBG is a reservoir of BTSC, a long-term culture of mixed PBG-constituting cells together with other cells may affect the phenotype of BTSC. Therefore, the nature of intact PBGs remains unclear. To solve these problems, I attempted to establish a method for isolating PBG-constituting cells from EHBD by FACS.

In the present study, I show that Trop2 is differentially expressed in EHBD. By using anti-Trop2 antibody, I isolated PBG-constituting cells to investigate their character by gene expression analysis and *in vitro* culture. Furthermore, I investigated the expression profile of Trop2 in EHBD after severe biliary injury model. With these results, I demonstrate that Trop2 is a useful marker for investigating the homeostatic and pathophysiological role of PBGs in EHBD.

Materials and methods

Animal models

C57BL/6J mice (CLEA Japan, Tokyo, Japan) were housed in a specific pathogen free animal facility under a 12 h dark/light cycle and provided with food and water ad libitum. Both male and female mice were used for this work. For bile duct ligation (BDL), mice at 8 weeks of age underwent anesthesia by the isoflurane (AbbVie, Tokyo, Japan) inhalation, and subcostal incision. The common bile duct (CBD) was ligated with a suture thread (4-0 VICRYL; Ethicon, Somerville, NJ) at the distal end of CBD. After abdominal closure by suture, mice were placed in a recovery cage until they regained consciousness. For the 5-bromo-2´-deoxyuridine (BrdU) incorporation assay, 3.75 mg of BrdU (Sigma-Aldrich, St. Louis, MO) was injected into the peritoneal cavity 2 h before sampling. All mouse studies were conducted in accordance with institutional procedures and approved by the Animal Care and Use committee of the Institute of Molecular and Cellular Biosciences, The University of Tokyo (approval numbers 2609, 2706, 2804 and 2904) and for the National Center for Global Health and Medicine Research Institute (approval number 17086).

Preparation of mouse tissue sample

Adult mouse tissue was mounted in O.C.T. compound (Sakura Finetek Japan, Tokyo, Japan) directly or after fixation with phosphate-buffered saline (PBS) containing 4% paraformaldehyde (PFA) overnight at 4˚C. In the case of

4% PFA fixation, the sample was washed with PBS for 10 min at room temperature (RT), and then placed in a series of sucrose dilutions at 4˚C. The concentration of sucrose in PBS was gradually elevated as follows: 10% for 4 h, 15% for 4 h and 20% overnight. Finally, the tissue was mounted in O.C.T. compound.

Visualization of mouse biliary tree

Visualization of whole mouse biliary system was performed by injection of black carbon ink from the duodenum. Following ink injection, liver and EHBD were gradually dehydrated by ethanol and immersed in benzyl alcohol/benzyl benzoate (BABB) optical clearing reagent (Kaneko et al., 2015).

Immunostaining of mouse tissue samples

Frozen sections (8 μm) were permeabilized with 0.2% Triton-X-100 in PBS. In case of sections of unfixed sample, I performed 4% PFA fixation at RT before permeabilization. Subsequently, sections were blocked with blocking buffer (5% skim milk in PBS) for 1 h at RT and incubated with diluted primary antibody overnight at 4˚C. Then, the sample was incubated with secondary antibody for 2 h at RT. To detect BrdU signal, sections were autoclaved in Tris-EDTA (TE) buffer (pH 8.0) for 5 min before permeabilization. Following autoclave treatment, sections were stained as described above. For whole-mount immunostaining, CBD was fixed with 4% PFA overnight at 4˚C and immersed in blocking buffer

(10% BSA and 1% Triotn-X-100 in PBS) overnight at 4˚C. Subsequently, the sample was incubated with diluted primary and secondary antibody overnight at 4˚C. Finally, optical clearing was performed by SeeDB overnight at RT (Ke et al., 2013). For the immunostaining of *in vitro* samples, I applied the same protocol as frozen sections. For staining cystic-organoids, I used the same reagents as whole-mount immunostaining. In all immunostaining, nuclei were stained with Hoechst 33342 (Sigma-Aldrich). Images were captured using Axio observer Z.1 with AxioCam HRc (Carl Zeiss, Jena, Germany), FV1200 and FV3000 (Olympus, Tokyo, Japan). Primary and secondary antibodies are listed in Table 4.

Flow cytometric (FCM) analysis and cell isolation

For isolation of mouse IHBD by flow cytometry, liver cells were prepared by collagenase digestion as previously described (Okabe et al., 2009). For preparation of EHBD cells, mouse CBD was surgically resected and incubated in the liver perfusion medium (Thermo Fisher Scientific, Waltham, MA) for 10 min at 37˚C after rinsing with 2 or 3% FBS-containing ice-cold PBS. After centrifugation at 1200 rpm for 3 min, the pellet was incubated in digestion medium (0.5 mg/ml Collagenase [Sigma-Aldrich], 0.5 mg/ml Pronase [Roche, Basel, Switzerland] and 0.25 mg/ml DNase1 [Sigma-Aldrich] in liver digestion medium [Okabe et al., 2011]) for 30-50 min at 37˚C. The dissociated cells were passed through a 70 μm cell strainer (Corning, Corning, NY) and centrifuged at 1500 rpm for 5 min. The cell pellet was resuspended with 2 or 3%

FBS-containing PBS and incubated with anti-Fc receptor antibody for 20 min on ice. After incubation with primary antibody for 30 min on ice, primary antibodies were washed out with 2 or 3% FBS-containing PBS. After centrifugation at 1500 rpm for 5 min, the cell pellet was incubated with secondary antibody for 20 min on ice. To exclude dead cells, propidium iodide (PI) was added before flow cytometric analysis. For cultured cells, the dissociated cells after incubation with Accutase (Thermo Fisher Scientific) for 40 min were stained in a similar manner. For analysis of apoptotic and necrotic cell death, I used the MEBCYTO Apoptosis Kit (MBL, Aichi, Japan) according to the manufacturer's protocol after washing secondary antibody away. The stained cells were analyzed by BD FACSCanto Ⅱ (BD Biosciences, Franklin Lakes, NJ) and sorted by Moflo XDP (Beckmann courter, Brea, CA). The antibodies used in this study are listed in Table 4.

Cell culture

For 2D culture, the isolated LBECs and PBECs were cultured on type I collagen-coated cell culture dish (Corning). The used medium is described in Table 5. Medium was changed every 3 days.

For the cyst formation assay, 3,000 isolated LBECs and PBECs were seeded on the gel mixture consisting (1:1) of the type I collagen (Nitta gelatin, Osaka, Japan) and growth factor reduced matrigel (BD Biosciences) in 8-well cover glass chamber (Thermo Fisher Scientific). Then, DMEMF medium (Wako

Pure Chemical Industries, Osaka, Japan) containing growth factor reduced matrigel (BD Biosciences), EGF and HGF was overlaid and cultured for 7 days (Tanimizu et al., 2014). For organoid culture, isolated PBECs were suspended in 50 μL growth factor reduced matrigel (BD Biosciences) and kept at 37˚C for 30 min in a 5% CO_2 incubator. Then, the medium was overlaid on the gel (Huch et al., 2013b). The composition of medium is described in Table 6.

Colony and cyst formation assay

For the colony formation assay, 1,000 or 3,000 isolated LBECs and PBECs were cultured for 6 or 8 days on the type I collagen-coated dishes (Corning) with a diameter of 60 mm. For the cyst formation assay, 3,000 isolated LBECs and PBECs were cultured for 7 days on a 8 well cover glass chamber (Thermo Fisher Scientific). After culture, the colonies or cysts were stained with Giemsa's solution (Merck Millipore, Burlington, MA) and imaged by IX-83 with DP80 (Olympus). The number of colony and cyst was counted by ImageJ cell counter tool.

Rhodamine123 incorporation assay

The incorporation of Rhodamine123 into cystic-organoid at culture day 11 was evaluated as previously reported (Sampaziotis et al., 2015). In this study, 100 μM Rhodamine123 (Sigma-Aldrich) was used for incorporation. For inhibition of multi drug resistance protein (Mdr), the cystic-organoid was

pretreated with 100 μM R-(+)-verapamil (Sigma-Aldrich) before Rhodamine123 incubation. Time laps imaging was performed by FV3000 with stage top CO2 incubator (TOKAI HIT, Shizuoka, Japan). Images were acquired every 2 min for 90 min.

Extraction of total RNA and cDNA synthesis

Extraction of total RNA from each sample was performed by using TRizol reagent (Thermo Fisher Scientific) or RNeasy micro kit (QIAGEN, Hilden, Germany). Genomic DNA was degraded with DNase I (Thermo Fisher Scientific and QIAGEN) during extraction step. The extracted total RNA was reverse-transcribed into cDNA with Primescript RT master mix (TaKaRa Bio, Shiga, Japan). The cDNA sample was subjected to RNaseH (Thermo Fisher Scientific) to degrade residual template RNA and analyzed by qRT-PCR analysis.

qRT-PCR

Gene expression analysis was performed with TaqMan universal probe system (Roche). Measurement of the signal was performed by LC96 (Roche). β-actin was used as an internal control (Roche, #05046190001). The information of primer and probe is listed in Table 7.

Microarray analysis

I compared the difference of gene expression pattern between isolated PBEC and LBEC by microarray analysis. Total RNA was extracted by RNeasy micro kit (Qiagen). Extracted total RNA was reverse-transcribed into cDNA and labeled cRNA was synthesized by TaKaRa Bio Inc. Labeled cRNA was analyzed by Agilent expression array analysis (TaKaRa Bio).

Statistical analyses and graphing

I compared the statistical difference between two groups by student t test, Welch's t test or Mann–Whitney U test. When comparing three-groups, I used Kruskal-Wallis test, with Dunn's multiple comparison test. Statistical significance was set at two-tailed *P* values < 0.05. Determination of the statistical test was based on the result of Shapiro-Wilk normality test and variance analysis. Statistical test and graphing were performed by R and Prism6 software.

Results

Lack of markers to distinguish mouse PBG from EHBD.

To identify PBG in mouse EHBD, we examined the expression profiles of several candidate molecules, which make it possible to distinguish between PBECs and LBECs. Because it is well known that cytokeratin 19 (CK19), EpCAM, osteopontin (Opn) and cystic fibrosis transmembrane conductance regulator (Cftr) are expressed in mouse IHBD, I first investigated the expression of these markers in EHBD. The immunohistochemical analysis of cross sections demonstrated that all of these markers were expressed in both the lumen and PBG of EHBD, indicating that EpCAM is applicable for purifying both PBECs and LBECs from the tissue of EHBD (Figure 8). However, another marker was required to distinguish between PBECs and LBECs. Because PDX1 is a marker characteristic of human BTSCs but not LPCs, I examined the expression of Pdx1 in mouse EHBD as well as IHBD. To avoid the contamination of IHBD to EHBD, I used a portion of the CBD as an EHBD sample for further analysis (Figure 9A). First, I isolated IHBD from the liver and BECs form EHBD by FACS using anti-EpCAM antibody (Figure 9B). Gene expression analysis revealed that *Pdx1* was predominantly expressed in BECs isolated from EHBD, but not detected in those from IHBD (Figure 10A). Consistently, immunohistochemical analysis of liver sections showed no expression of Pdx1 in IHBD (Figure 10B). To determine the localization of Pdx1 in EHBD, I visualized EHBD by whole-mount immunostaining after optical clearing (Figure 11A). The sagittal images of EHBD

stained with anti-EpCAM and anti-Pdx1 antibodies by confocal microscopy showed that Pdx1 was expressed in both the luminal epithelium and PBG of EHBD (Figure 11B), which is consistent with previously reported expression patterns (Fukuda et al., 2006; Dipaola et al., 2013). Similarly, the staining of Sox9 (Figure 11C), a transcription factor for LPCs (Furuyama et al., 2011), was unable to discriminate PBGs from EHBD. Therefore, these molecules are insufficient to define the identity of PBECs in mouse EHBD.

Trop2 is predominantly expressed in LBECs, but not in PBECs.

Trop2 has been previously identified as a stem/progenitor cell marker for the liver as well as the prostate. (Goldstein et al., 2008; Okabe et al., 2009). However, the expression profile of Trop2 in EHBD has not been reported previously. I therefore analyzed *Trop2* expression in $EpCAM^+$ BECs isolated from EHBD and IHBD by qRT-PCR. Strikingly, *Trop2* was expressed in BECs derived from EHBD but not in those from IHBD (Figure 12). Further FCM analysis revealed that EHBD-derived $EpCAM^+$ BECs could be subdivided into $Trop2^+$ and $Trop2^-$ fractions (Figure 13A). To clarify which type of $EpCAM^+$ BECs express Trop2 in EHBD, I performed whole-mount immunostaining using antibodies against Trop2 and EpCAM. Surprisingly, I found that Trop2 was predominantly expressed in the lumen of EHBD, but not in PBG (Figure 13B). From these results, I hypothesized that Trop2 is a specific cell surface marker to identify the lumen of EHBD, and that $EpCAM^+Trop2^+$ and $EpCAM^+Trop2^-$ BECs

correspond to LBECs and PBECs, respectively.

Trop2^{+} BECs show PBG-like characteristics.

To confirm whether Trop2 is able to separate LBECs and PBECs, I compared gene expression related to PBGs and/or BTSCs between freshly isolated Trop2^{+} and Trop2^{-} BECs (Figure 14 and 15). It has been reported that chromogranin A (ChgA) and LGR5 are expressed in mouse and human PBGs, respectively (Carpino et al., 2012; Dipaola et al., 2013; Lanzoni et al., 2016). In addition, it has been reported that human PBGs contain epithelial cells secreting several pancreatic enzymes such as α-amylase isozymes, trypsin and pancreatic lipase (Terada et al. 1993). Consistent with these previous reports, both *ChgA* and *Lgr5* were expressed in Trop2^{-} BECs, while the expression of these genes was negligible in Trop2^{+} BECs (Figure 16). Notably, several pancreatic molecules such as *somatostatin* (*Sst*), *pancreatic lipase* (*Pnlip*) and *amylase2a5* (*Amy2a5*) were detected in Trop2^{-} BECs, while these expression levels were negligible in Trop2^{+} BECs (Figure 16). Consistent with the notion that PBGs include mucinous acini, high expression of *mucin 6, gastric* (*Muc6*) was also detected in Trop2^{-} BECs compared with Trop2^{+} BECs (Figure 16). In contrast, most of conventional BEC markers such as *CK19*, *Epcam*, *Cftr* and *anion exchanger protein 2* (*Ae2*) were equally expressed in both Trop2^{-} and Trop2^{+} BECs (Figure 17), consistent with the immunohistological data of mouse EHBD (Figure 8) and rat EHBD (Venter et al., 2015). These results supported

the hypothesis that Trop2 is a valuable cell surface marker to distinguish the luminal epithelium from PBGs of EHBD, i.e. LBECs and PBECs.

PBECs express makers of tissue stem/progenitor cell in the gastrointestinal compartment.

To investigate difference between LBECs and PBECs, I then compared gene expression profile of isolated LBECs and PBECs by microarray analysis (Figure 14). Consistent with qRT-PCR data, PBECs expressed Trop2 and human PBGs related genes at higher levels (Table 8). Moreover, PBECs also expressed *doublecortin like kinase* (*Dclk1*), a marker of the intestinal tuft cell located in the intestinal crypt (Nakanishi et al., 2013) (Table 8).

Interestingly, PBECs showed higher gene expression of pancreatic and endocrine progenitor cell markers such as *glycoprotein 2* (*GP2*) and *delta/notch like EGF repeat containing* (*Dner*) (Hald et al., 2012; Cogger et al., 2017) and intestinal stem/progenitor cell markers such as *olfactomedin 4* [*Olfm4*] and *achaete-scute family bHLH transcription factor 2* [*Ascl2*]) (van der Flier et al., 2009a, b) (Table 9). These results supported the hypothesis that PBGs contain tissue stem/progenitor cells. Human BTSCs also express pluripotent-related genes such as *Oct4*, *Sox2* and *Nanog* (Carpino et al., 2012; Cardinale et al., 2012; Lanzoni et al., 2016). However, there was no difference in these gene expressions between mouse isolated PBECs and LBECs (Table 9).

PBECs show higher colony forming activity than LBECs.

Because PBECs showed a gene expression pattern similar to tissue stem/progenitor cells, I isolated each cell fraction by FACS and performed *in vitro* colony formation assay (Figure 14). Interestingly, PBECs showed significantly higher colony formation capacity than LBECs in the primary culture (Figure 18). Combining with gene expression analysis, I hypothesized that PBGs contain more stem/progenitor-like cells.

PBECs show LBEC-like phenotype in the 2D culture condition.

To further characterize the expanded cells derived from PBECs, I investigated the expression of several EHBD markers by immunocytochemical and FCM analyses. Isolated PBECs expanded on the dish (Figure 19). Immunostaining of cultured PBECs revealed that the expression of EpCAM, CK19, Sox9 and Pdx1 was maintained after 6 days of culture (Figure 20). More interestingly, most cultured PBECs expressed Trop2, although it was hardly detected in PBECs at the beginning of culture (Figure 15 and 21). The induction of Trop2 expression in cultured PBECs was confirmed by qRT-PCR, immunostaining and FCM analysis (Figure 21). In contrast to Trop2 expression, downregulation of *ChgA*, *Sst, Muc6* and *Lgr5* was observed (Figure 22), suggesting that PBECs gave rise to the cells characteristic of LBECs concomitantly with the expansion on the dish.

PBECs form luminal structures in the 3D culture condition.

Because PBECs showed high potential for colony formation composed of LBEC-like cells, I next examined bile duct-forming capacity of PBECs. As previously reported, the potential of BECs can be evaluated by the formation of cysts with luminal epithelial polarity in the 3D culture (Tanimizu et al., 2014). I thereby compared cyst formation capacity between PBECs and LBECs. Similar to colony formation assay, PBECs showed significantly higher cyst formation capacity than LBECs (Figure 23), suggesting that PBECs contain more progenitor-like cells with a potential to form bile ducts. However, this culture condition did not seem to be suitable for further analysis of PBECs, because it was not adapted for long-term culture of PBECs, resulting in arrest of the growth of cysts. Therefore, I applied another 3D organoid culture system previously reported by Clevers's group to isolated PBECs (Huch et al., 2013b). After 5 days of culture, PBECs formed apparently spherical cystic-organoids that grew progressively (Figure 24). Dual staining of CK19 and Ki67 revealed that the cystic organoids were formed mainly by the proliferation of PBECs rather than their aggregation (Figure 25). After 10 days of culture, I investigated whether the cystic-organoids exhibited epithelial cell polarity by evaluating the localization of the apical (F-actin) and basolateral (integrin alpha 6 [ITGA6]) markers. Expectedly, F-actin was localized in the apical membrane of the cyst-forming cells, while ITGA6 was localized in the basolateral compartment (Figure 2-26), indicating the proper polarity of luminal epithelium. In addition, qRT-PCR and

immunostaining of Trop2 demonstrated that cystic-organoids were composed of Trop2^{+} cells, similarly to the luminal epithelium of EHBD *in vivo* (Figure 27). Consistently, gene expression analysis by qRT-PCR showed downregulation of *ChgA*, *Sst* and *Muc6* in the proliferating organoid-forming cells (Figure 28), suggesting that PBEC has a potential to produce LBEC-like cells with the luminal structure. In contrast, *Lgr5* was not downregulated under this 3D culture condition unlike the 2D culture condition (Figure 28). Furthermore, I investigated whether the formed luminal structure is functionally similar to *in vivo* bile ducts. One of the known functions of bile ducts is to regulate bile homeostasis by transportation of water and ions via transmembrane channels such as multidrug-resistance protein 1 (Mdr1) (Gigliozzi et al., 2000). Recently, Sampaziotis and colleagues have reported that human EHBD-derived organoids show Mdr1 dependent secretory function (Sampaziotis et al., 2017). Therefore, we examined whether PBEC-derived cystic-organoids have Mdr1 dependent secretory capacity by the incorporation of Rhodamine123, a substrate of Mdr1. As a result, the gradual accumulation of Rhodamine123 was observed in the luminal space of cystic-organoids, whereas it was blocked in the presence of verapamil, a Mdr antagonist (Figure 29). From these results, I hypothesized that PBECs have a potential to differentiate into functional LBECs.

Trop2 expression in PBG dramatically changes by biliary injury.

It has been previously reported that severe damage to the biliary tree such

as by BDL induces the proliferation of EHBD (Dipaola et al., 2013). However, the nature of PBG during regeneration remains unclear. As shown in Figure 30, hematoxylin-eosin (H&E) staining of EHBD after BDL showed remarkable dilation of the lumen accompanied by the detachment of epithelium after 7 days of BDL. Although EHBD did not exhibit apparent cellular damage 2 days after BDL by H&E staining, FCM analysis of EHBD using Annexin V and propidium iodide (PI) revealed that apoptosis and necrosis of EHBD increased remarkably at this time point (Figure 31). Next, I performed dual staining of Ki67 and CK19 in EHBD to investigate the extent of regeneration in LBECs and PBECs. Although intense signal of Ki67 was detected in PBG before biliary injury, it was observed at the apical membrane of PBECs rather than nucleus (Figure 32B), suggesting that this staining is non-specific. The idea was further supported by no incorporation of BrdU in PBG before injury (Figure 32C). In contrast, many LBECs and PBECs showed nuclear staining of Ki67 after BDL and then the ratio of $Ki67^+$ cells in the luminal epithelium and PBG gradually decreased, suggesting that LBECs and PBECs are capable of proliferating upon biliary insult (Figure 32A). More interestingly, Trop2 was expressed in most of PBECs 2 days after BDL (Figure 33A). Consistent with the immunohistological data, FCM analysis showed that the ratio of $Trop2^+$ cells in $EpCAM^+$ BECs rapidly increased after BDL (Figure 33B). These results suggested that PBECs activated by biliary damage may give rise to the luminal $Trop2^+$ BECs for the bile duct regeneration as observed by using *in vitro* colony and organoid formation assay. I therefore

isolated Trop2^{+} and Trop2^{-} BECs after BDL (Figure 34) to compare their colony formation capacity. As shown in Figure 35, the capacity for colony formation in Trop2^{+} BECs was dramatically increased after BDL. Considering that Trop2^{-} PBECs exhibited higher colony formation capacity than Trop2^{+} LBECs isolated from non-treated (NT) EHBD (Figure 18 and 35) and that Trop2 expression was rapidly induced in PBGs after BDL, PBEC-derived Trop2^{+} cells may account for the remarkable increase of colony formation capacity in Trop2^{+} BECs after BDL, rather than the phenotypic change of Trop2^{+} LBEC. In contrast, a small population of Trop2^{-} BECs remained in EHBD even after BDL (Figure 33 and 34). However, the colony formation capacity of Trop2^{-} BECs was decreased after 7 days of BDL, presumably due to exhaustion of the stem/progenitor cell compartment or fatal damage by prolonged injury (Figure 35).

Discussion

Since the discovery of PBGs associated with the biliary tree in humans, the anatomical and histochemical studies have mainly been performed using human samples. It has been reported that PBGs are tubuloalveolar glands with mucinous and serous glandular acini composed of heterogeneous cell compartments. The expression of a variety of secretory factors including mucins, neuroendocrine protein (e.g. ChgA) and pancreatic enzymes (e.g. α-amylase, trypsin, and lipase) has been reported in adult PBGs in healthy and diseased states (Terada et al., 1993; Dipaola et al., 2013). The structure of PBG in EHBD is reminiscent of the crypt structures of the intestine and stomach (Figure 36). In contrast to numerous studies on the localization and differentiation status of crypt-forming component cells in the gastrointestinal system, the nature of PBGs in EHBD remains uninvestigated and poorly understood. In addition, the similarity and difference of PBECs between human and mouse also remains unclear. In the present study, I have demonstrated that Trop2 is differentially expressed between the luminal epithelium and PBG of EHBD and that Trop2 expression is applicable for FACS-based separation of each cell component. The gene expression analysis of LBECs and PBECs derived from mouse EHBD revealed that the expression of neuroendocrine proteins (e.g. *ChgA*) and pancreatic markers (e.g. *Amy2a5*, *Sst* and *Pnlip*) and mucin (*Muc6*) was exclusively detected in the PBECs fraction, consistent with the previous reports about human PBGs. Although several human BTSC markers (e.g. EpCAM,

Sox9 and Pdx1) were expressed in both LBECs and PBECs in mice, Lgr5 was differentially expressed in the PBEC fraction (Figure 16), suggesting that Lgr5 might be a better marker for characterization of BTSCs in mice. Further analysis of gene expression in PBECs may provide useful clues as to how the extrahepatic biliary system is constructed by various types of component cells.

Since Cardinale and colleagues reported that multipotent stem/progenitor cells capable of differentiating into hepatocytes, BECs and pancreatic islets are present in the human extrahepatic biliary tree (Cardinale et al., 2011), PBG has been suggested to be a reservoir of BTSCs. Considering the location of multipotent stem/progenitor cells in PBGs, the physiological role of BTSCs may be involved in the maintenance or repair of the biliary epithelium in the vicinity of PBGs. In fact, it has been reported that the hyperplasia and the proliferation of PBGs occur in patients with hepatolithiasis, cholangitis and diabetes, as well as in rodent models of bile duct and pancreas injury (Table 3), although there is no direct evidence that PBGs contribute to regeneration of EHBD. In this study, I showed that PBECs isolated from normal EHBD contain highly proliferative progenitor-like cells with colony formation capacity *in vitro*, which can also form cysts with luminal epithelial polarity and Mdr1 dependent secretory function in the 3D organoid culture system. More importantly, the PBEC-derived organoids comprised of epithelial cells with gene expression profiles similar to LBEC, i.e. upregulation of *Trop2* and downregulation of *ChgA*, *Sst* and *Muc6*, suggesting that PBECs possess a potential of supplying LBEC. Consistently, I found that the

PBECs proliferated *in vivo* upon biliary damage by BDL, re-expressing Trop2 dramatically. Concomitantly, the $Trop2^{+}$ BECs isolated from EHBD 2 days after BDL showed colony formation capacity comparable to the $Trop2^{-}$ PBECs prior to biliary injury. From these *in vivo* and *in vitro* data, it is plausible that PBG plays a role as a source of regenerating biliary epithelial cells by giving rise to transit amplifying cells (Figure 2-37).

Trop2 was initially discovered as a marker of invasive trophoblasts and a molecule structurally related to paralogous EpCAM. The expression of these two related molecules has been described in various organs during development as well as tumorigenesis (Tsukahara et al., 2011; Trerotola et al., 2013; Mustata et al., 2013; Fernandez Vallone et al., 2016). Of note, Trop2 has been reported to be expressed in adult or fetal-type stem/progenitor cells in various organs (Goldstein et al., 2008; Okabe et al., 2009; Mustata et al., 2013; Fernandez Vallone et al., 2016). Goldstein and colleagues reported that Trop2 identifies a subpopulation of murine and human prostate basal cells with stem cell characteristics (Goldstein et al., 2008). Okabe and colleagues have reported previously that Trop2 is expressed in proliferating LPCs induced by DDC diet injury, while it is hardly detected in the liver at the steady state (Okabe et al., 2009). A similar observation has been reported in two recent papers that Trop2 is re-expressed or induced in adult regenerating gastric glands or remodeling airway epithelium after epithelial damage, while it is absent in normal tissues (Fernandez Vallone et al., 2016; Liu et al., 2016). In this study, I also showed that

Trop2 is up-regulated in PBGs after BDL while it seems to be absent in normal PBGs. All of these reports imply the role of Trop2 in the process of stem/progenitor cell-mediated organogenesis or regeneration. In fact, a variety of functions of Trop2 have been reported, including cell proliferation, differentiation, adhesion and migration (Wang et al., 2008; Tsukahara et al., 2011; Stoyanova et al., 2012). However, it should be noted that the present study is different from the above mentioned cases, because the luminal epithelium of normal EHBD expresses Trop2 constitutively. In the corneal epithelia, Trop2 has been reported to enhance the expression and localization of tight junctional proteins, including Claudin-1 and -7 (Nakatsukasa et al., 2010). Therefore, there is a possibility that Trop2 may play a role in reinforcing the barrier of EHBD to avoid the leakage of toxic bile. Thus, it remains unknown whether the upregulation of Trop2 in PBGs is a step in stem/progenitor cell activation or a process of differentiation into LBECs. Nonetheless, the drastic change of Trop2 expression as well as the colony and organoid formation capacity of PBECs showed the possibility that PBGs contribute to EHBD regeneration. Given that PBG is a niche for BTSC, multipotent hepatobiliary-pancreatic stem/progenitor cells in EHBD must be Trop2-negative. Considering that Trop2 is induced in LPCs, bipotential hepatobiliary progenitors in DDC-damaged liver, a mouse model of sclerosing cholangitis, the expression of Trop2 may account for the commitment of hepatic lineage. Although it remains unclear whether $Trop2^{+}$ BECs in injured PBGs are derived from BTSCs, they

may originate from PBECs by de-differentiation, similar to injured intestine and stomach. Further studies using genetic ablation or lineage tracing experiments will reveal functional role(s) for Trop2 and PBGs in tissue repair of the biliary tree as well as other organs.

Conclusions

PBG has attracted many researchers' attention as a potential reservoir for a tissue stem/progenitor cell. However, the lack of useful method for isolating PBECs has hampered the investigation of the nature of PBGs. In this study, I developed FACS-based method for EHBD cell identification and showed that Trop2 is a useful cell surface marker for isolation and characterization of PBECs at a single cell level. Moreover, the present study has revealed that PBEC shows tissue progenitor cell-like characteristics and dramatically changes its phenotype after EHBD injury. Thus, isolation and characterization of PBECs based on Trop2 expression will provide useful information as to the nature of BTSCs and reveal the role of PBG in the homeostasis and regeneration of EHBD.

Figures and tables

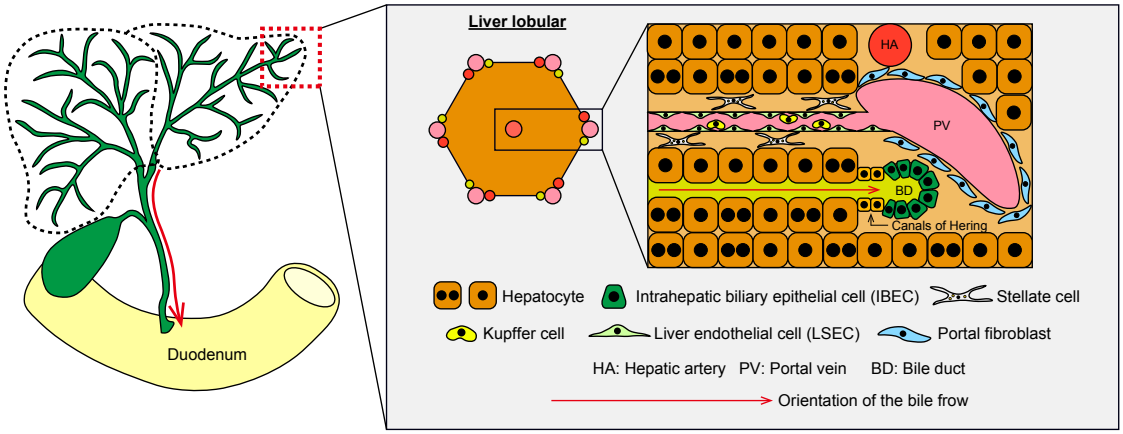

Figure 1. Schematic diagram of the liver architecture and component cells.

Liver is composed of many hepatic lobules and contains hepatocytes (parenchymal cell) and many kinds of hepatic non-parenchymal cells (NPCs). The portal triad is located in vertex of the hepatic lobule. Bile ducts drain bile into the duodenum. Red arrows indicate orientation of the bile flow.

IBEC: intrahepatic biliary epithelial cell, LSEC: liver endothelial cell, HA: hepatic artery, PV: portal vein, BD: bile duct.

A

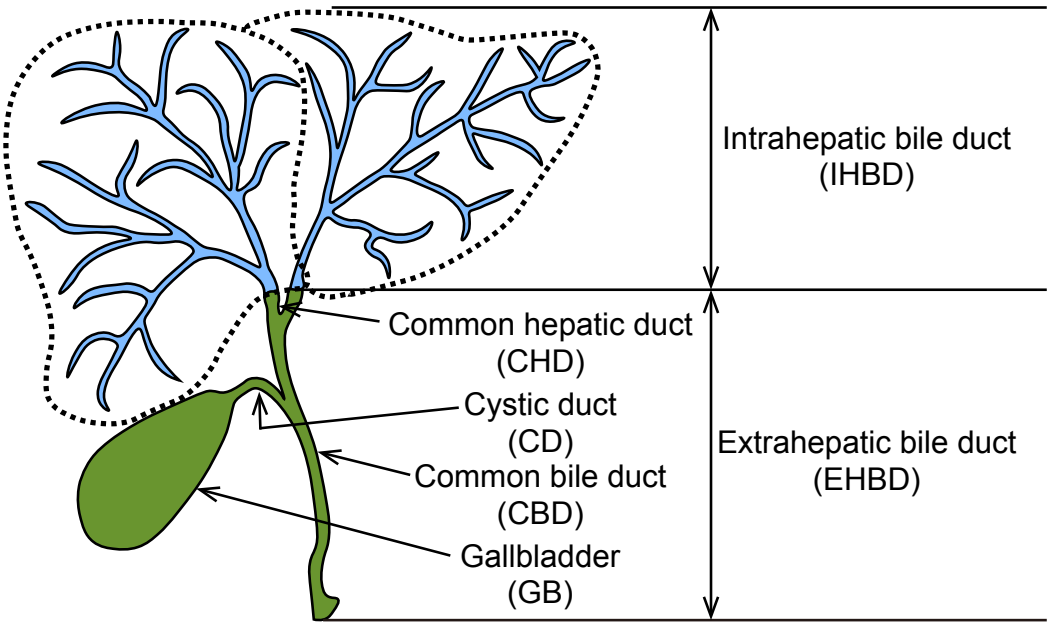
Intrahepatic bile duct
(IHBD)
Common hepatic duct
(CHD)
Cystic duct
(CD)
Common bile duct
(CBD)
Gallbladder
(GB)
Extrahepatic bile duct
(EHBD)

B

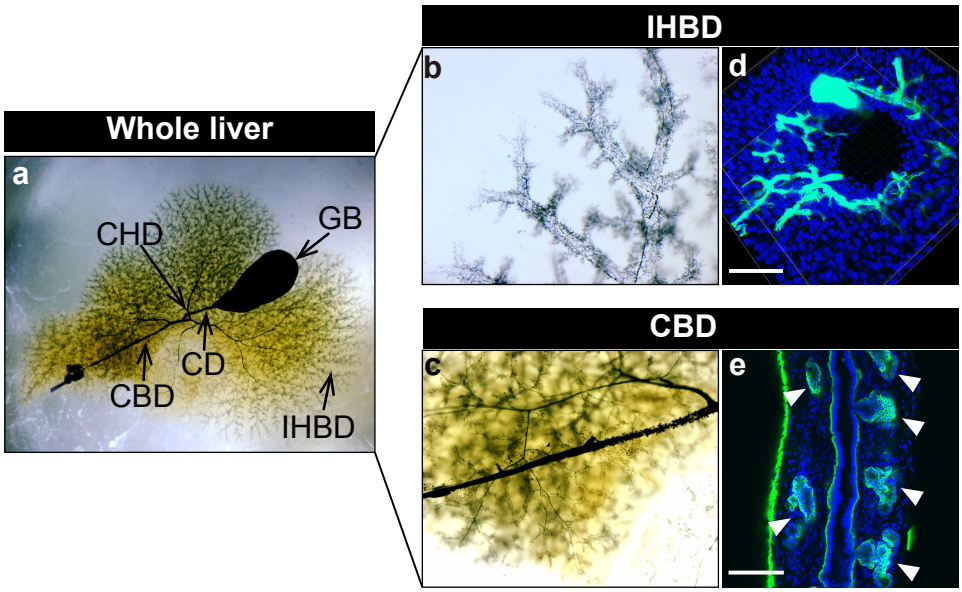
Whole liver
a
CHD
GB
CD
CBD
IHBD
IHBD
b
d
CBD
c
e

Figure 2. Structure of the biliary system.

(A) Schematic view of the biliary system. IHBD (blue) forms an intricate tree-like network in the liver parenchyma. EHBD (green) is composed of common hepatic duct (CHD), cystic duct (CD) common bile duct (CBD) and gallbladder (GB). (B) Visualization of the mouse biliary system by injection of black carbon ink (a-c) and immunostaining (d and e). IHBD and CBD were stained with anti-cytokeratin 19 (CK19) antibody. The optical clearing was performed in both imaging experiments. Arrowheads: Peribiliary glands (PBGs). Scale Bars = 100 μm.

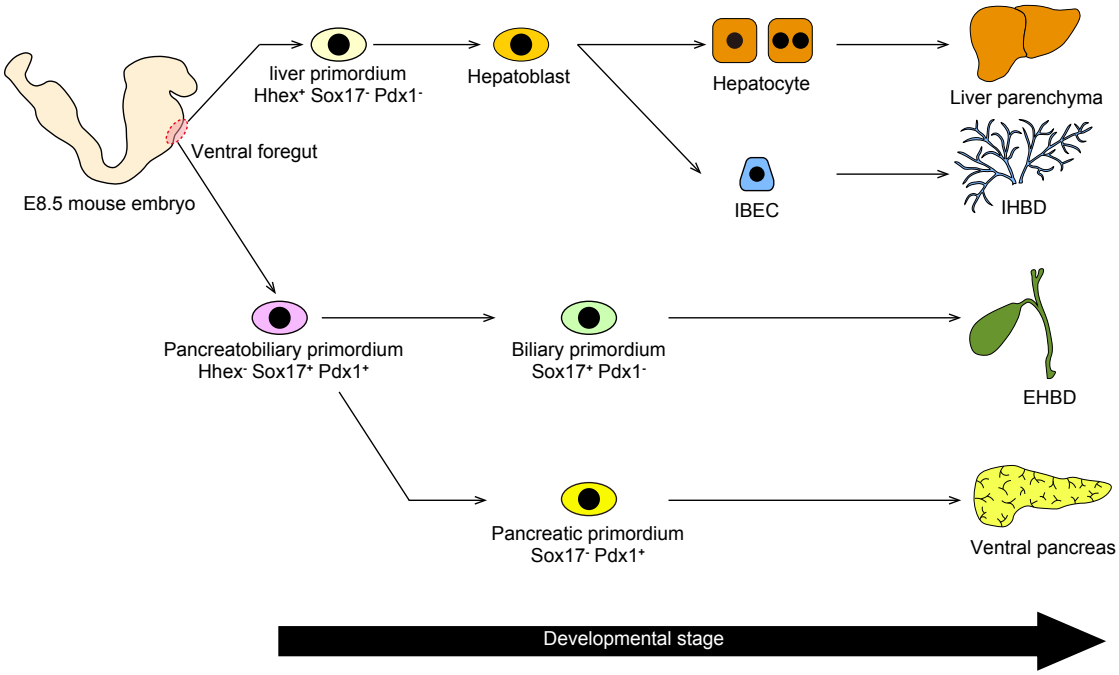

Figure 3. Schematic diagram of the mouse liver, extrahepatic biliary system and pancreas development.

Segregation of the liver (Hhex^{+} Sox17^{-} Pdx1^{-}) and the pancreatobiliary (Hhex^{-} Sox17^{+} Pdx1^{+}) lineage occurs at E8.5. At E10.5, the pancreatobiliary primordium is segregated into the biliary primordium (Sox17^{+} Pdx1^{-}) and the pancreatic primordium (Sox17^{-} Pdx1^{+}).

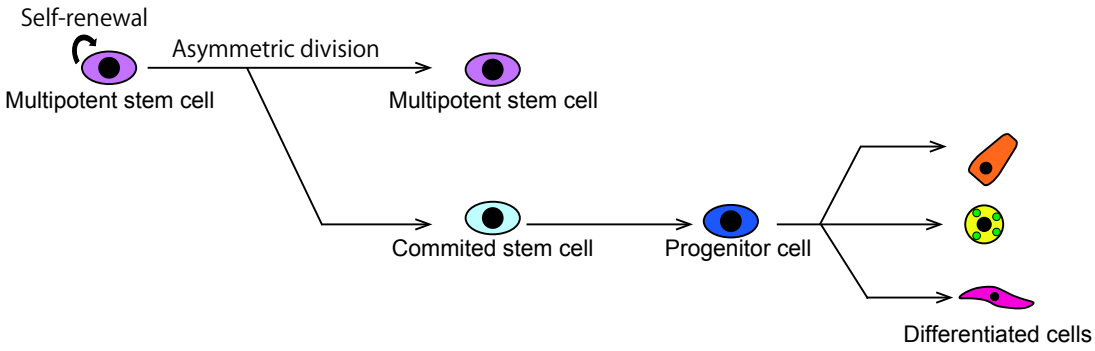

Figure 4. Schematic diagram of the stem cell system.

Multipotent stem cell supplies lineage committed stem cell and multipotent stem cell by asymmetric cell division. Lineage committed stem cell differentiates into functional progenies.

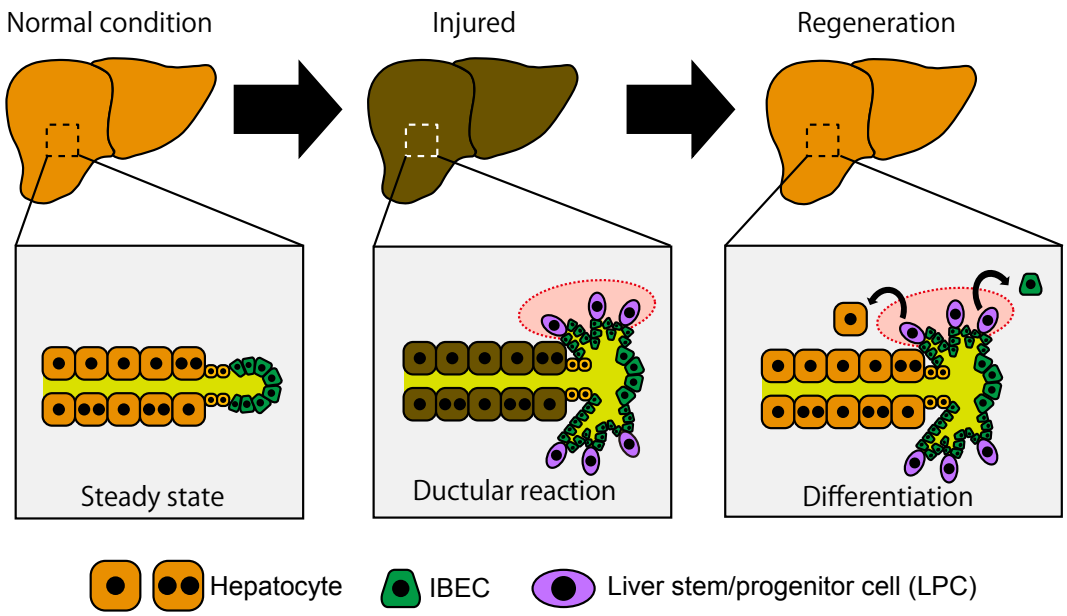

Figure 5. Schematic diagram of the LPC dependent liver regeneration.

When the liver is injured chronically or severely, liver stem/progenitor cells (LPCs) and IBECs proliferate and expand toward the damaged area (Ductular reaction). Expanded LPCs differentiate into functional hepatocytes and mature IBECs. Red dashed circles indicate the injured area.

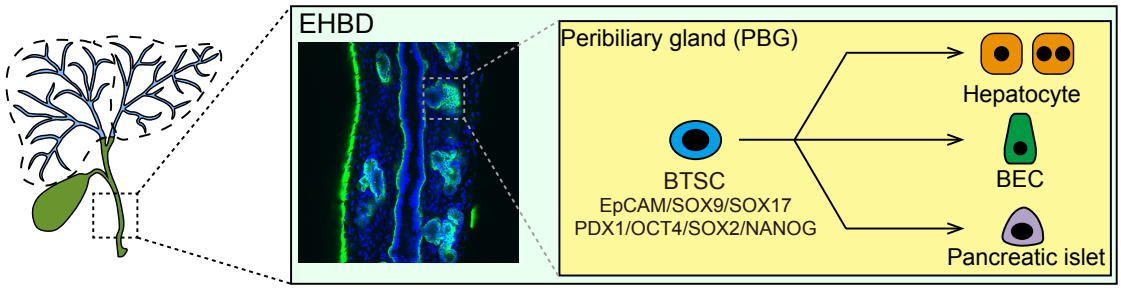

Figure 6. Schematic diagram of BTSCs.

BTSCs have been postulated to exist in PBGs and have a potential to differentiate into hepatocytes, mature BECs and pancreatic islets.

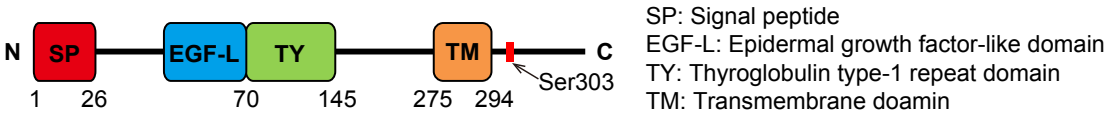

Figure 7. Domain structure of the Trop2.

Trop2 protein has a short signal peptide (SP), the epidermal growth factor-like domain (EGF-L) and the thyroglobulin type-1 repeat domain (TY) in the extracellular domain. On the other hand, Trop2 contains a PIP_2 binding site and a phosphorylation site (Ser 303) in the intracellular domain.

A

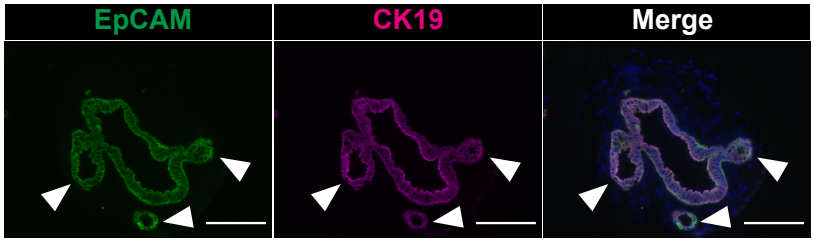

B

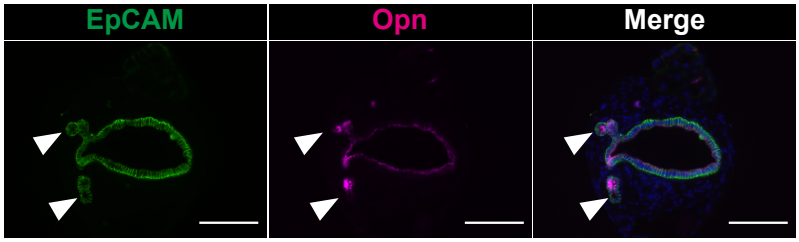

C

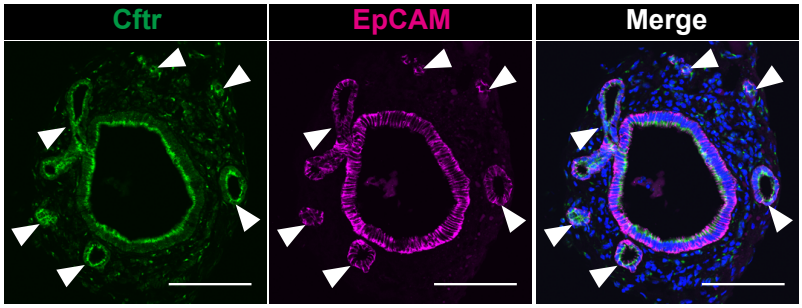

Figure 8. Expression of LPC markers in adult mouse EHBD.

(A-C) Immunohistochemical images of transverse sections of adult EHBD. Representative images stained with anti-EpCAM and anti-CK19 (A), anti-Opn (B) or anti-Cftr (C) antibodies are shown. Arrowheads indicate PBGs. Scale bars = 100 μm.

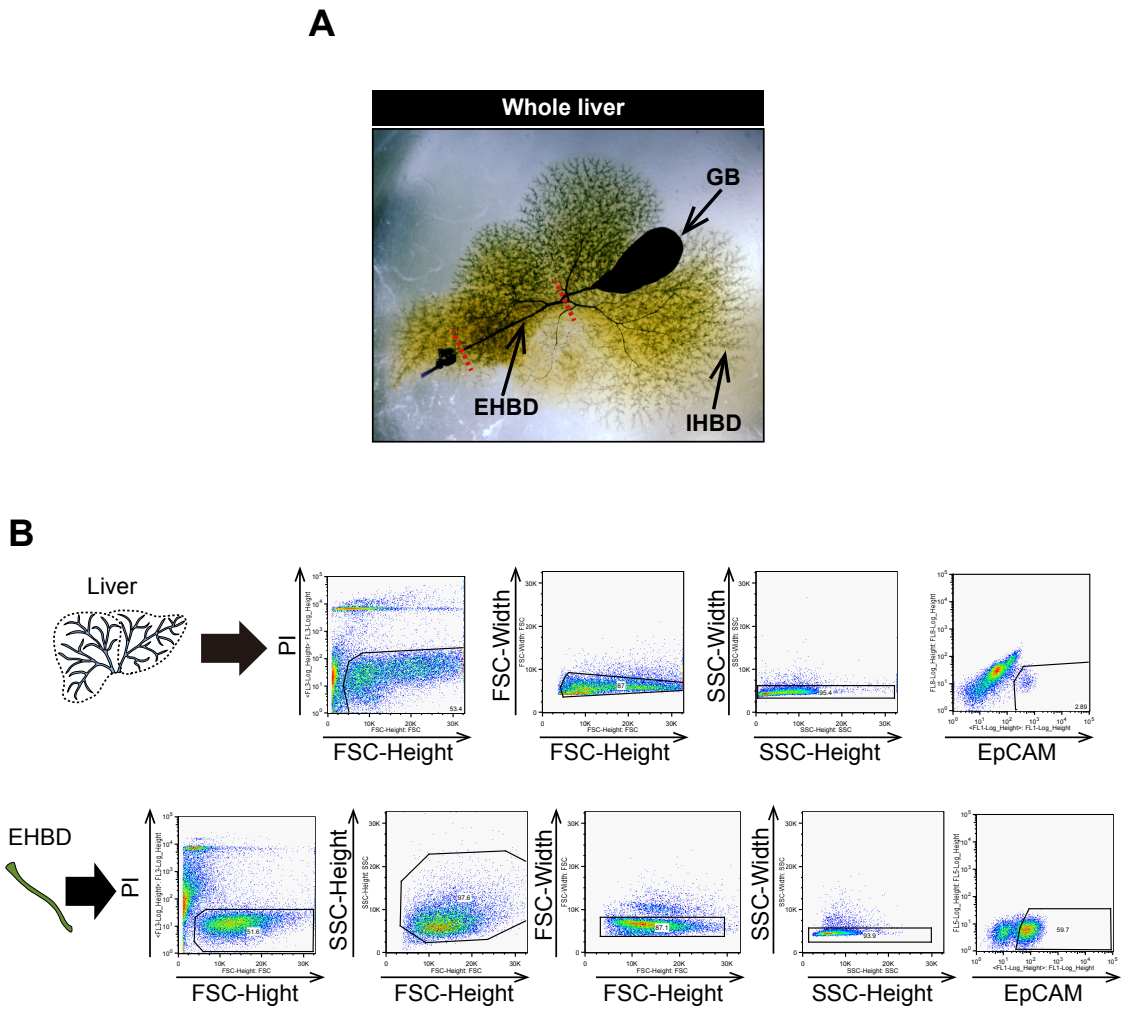

Figure 9. Isolation of IHBD and EHBD cells.

(A) Macroscopic image of the entire mouse biliary system. To show the portion used for this study, the biliary tree was visualized by injection of black carbon ink, followed by tissue clearing. The portion between red dotted lines was surgically resected and used as an EHBD sample. (B) Cell sorting of EpCAM^{+} BECs comprising IHBD and EHBD. After hepatic non-parenchymal cells (NPCs) or EHBD cells were stained with anti-EpCAM antibody, the gated cell fraction was recovered by FACS. FSC: forward scatter, SSC: side scatter, GB: gallbladder.

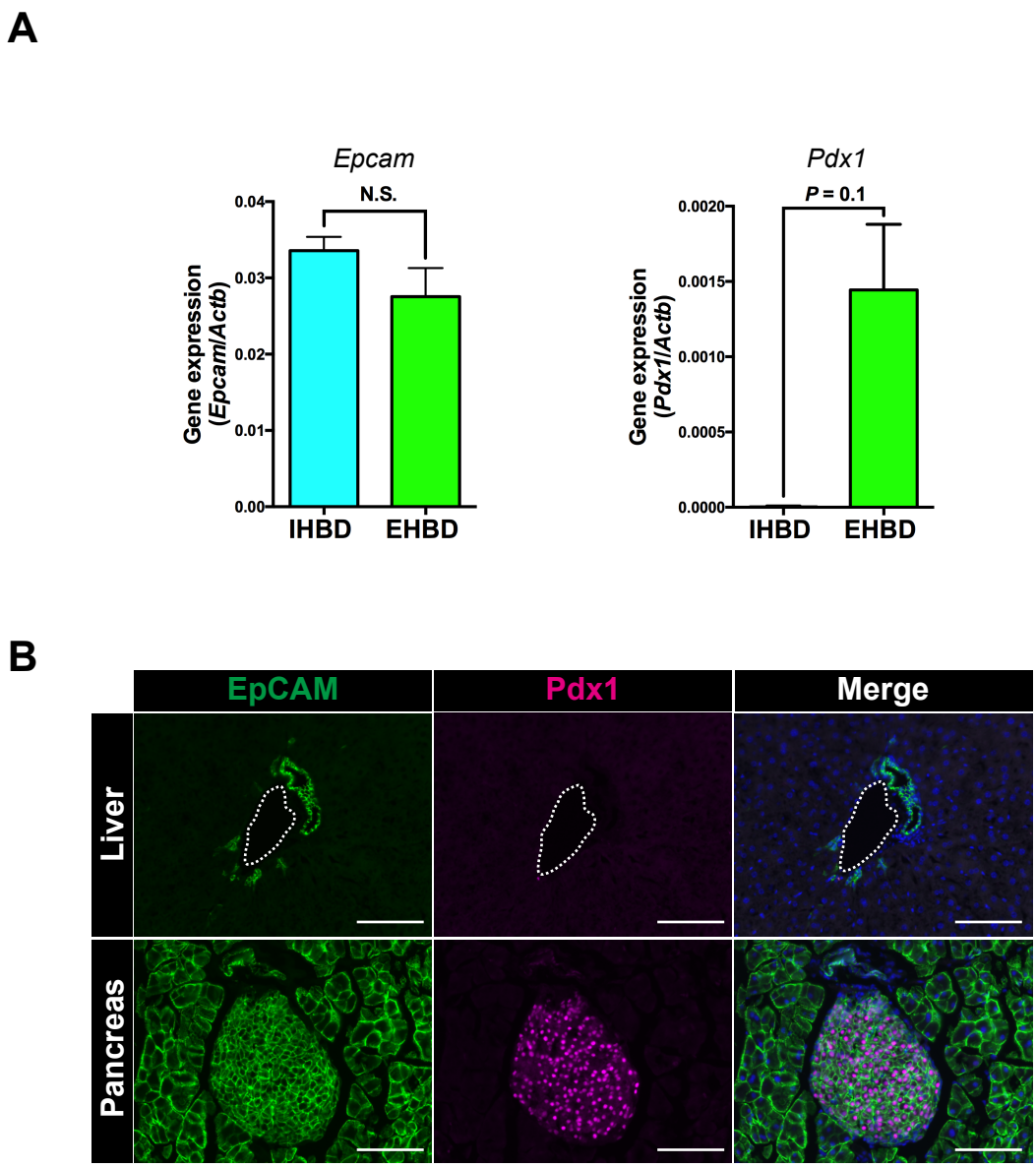

Figure 10. Expression analysis of the Pdx1 in isolated mouse EpCAM$^+$ EHBD and IHBD comprising BECs.

(A) Gene expression analysis of *Epcam* and *Pdx1* in BECs derived from IHBD and EHBD by qRT-PCR. Normalized values against *Actb* expression are shown as means ± SD (n = 3). N.S.: not significant. (B) Immunostaining of adult mouse liver and pancreas sections with anti-EpCAM and Pdx1 antibodies. Pancreas was used as a positive control for Pdx1 antibody. Dashed circle: PV. Scale bars = 100 μm.

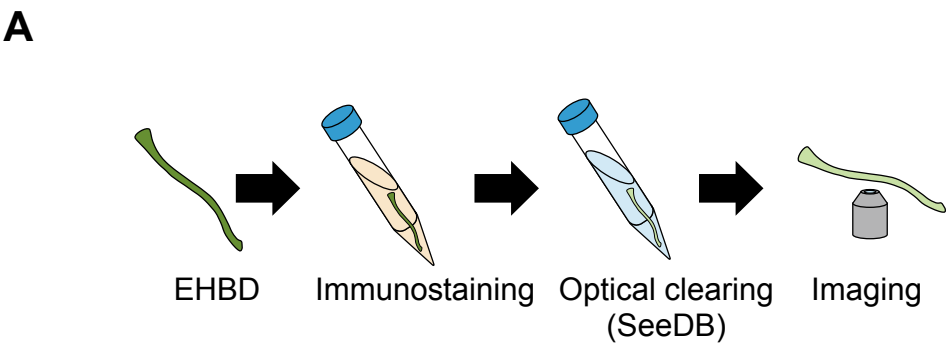

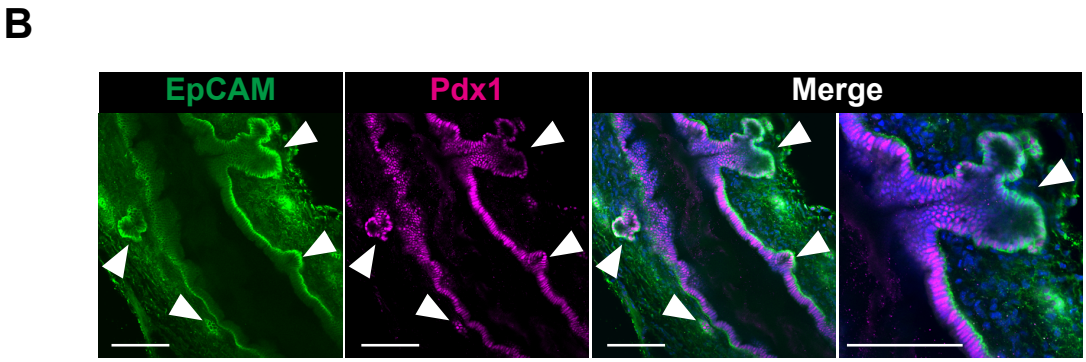

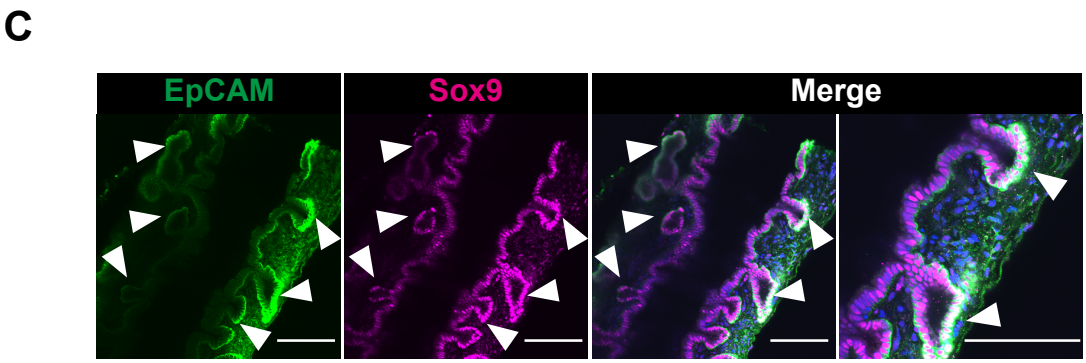

Figure 11. Expression analysis of the transcriptional factors for LPC and pancreatic progenitor cell.

(A) Experimental procedure of whole-mount immunostaining of EHBD. (B, C) Whole-mount immunostaining of EHBD after optical clearing. Representative sagittal images stained with anti-EpCAM and anti-Pdx1 (B) or anti-Sox9 (magenta) (C) are shown. Arrowheads: PBGs. Scale bars = 100 μm.

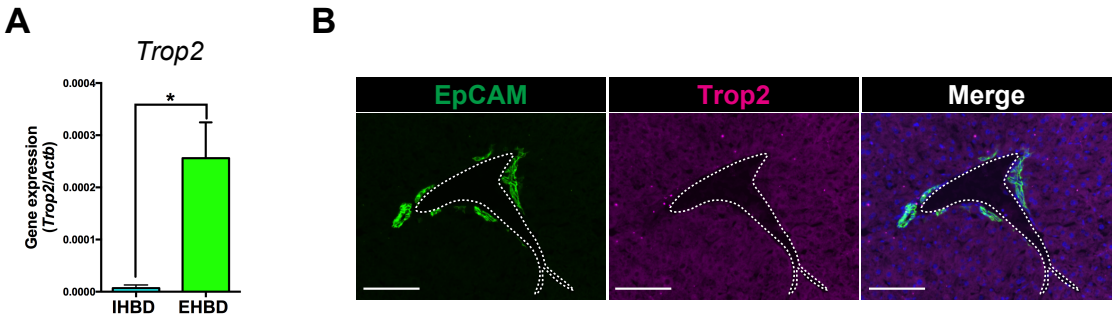

Figure 12. Expression analysis of Trop2 in isolated mouse EpCAM$^+$ EHBD and IHBD comprising BECs.

(A) Gene expression analysis of *Trop2* in BECs derived from IHBD and EHBD by qRT-PCR. Normalized values against *Actb* expression are shown as means ± SD (n = 3, **P* < 0.05). (B) Immunostaining of adult mouse liver sections with anti-EpCAM and Trop2 antibodies. Dashed circle: PV. Scale bars = 100 μm.

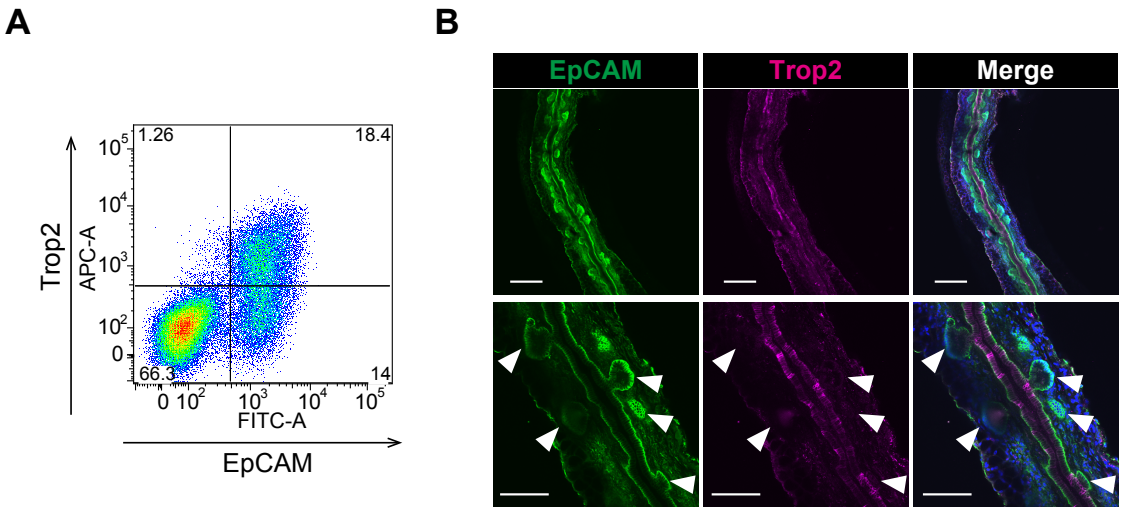

Figure 13. Expression of Trop2 in adult mouse EHBD.

(A) FCM analysis of EHBD with anti-EpCAM and anti-Trop2 antibodies. (B) Whole-mount immunostaining of EHBD using anti-EpCAM and anti-Trop2 antibodies. Arrowheads: PBGs. Scale bars = 200 μm (upper panel) and 100 μm (lower panel).

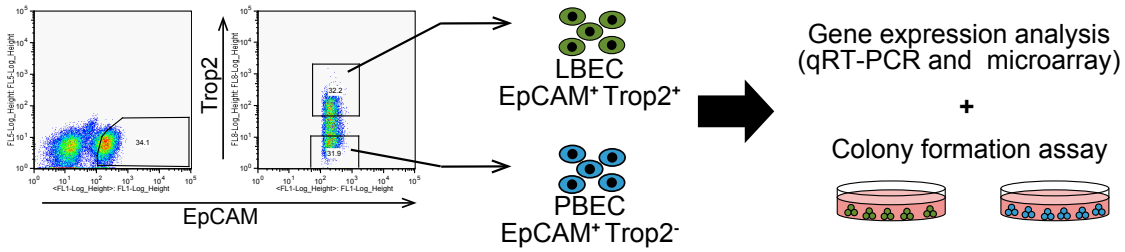

Figure 14. Experimental design for characterization of LBECs and PBECs.
LBECs (EpCAM$^+$ Trop2$^+$) and PBECs (EpCAM$^+$ Trop2$^-$) were isolated by FACS. Isolated LBECs and PBECs were characterized by qRT-PCR, microarray analysis and *in vitro* colony formation assay.

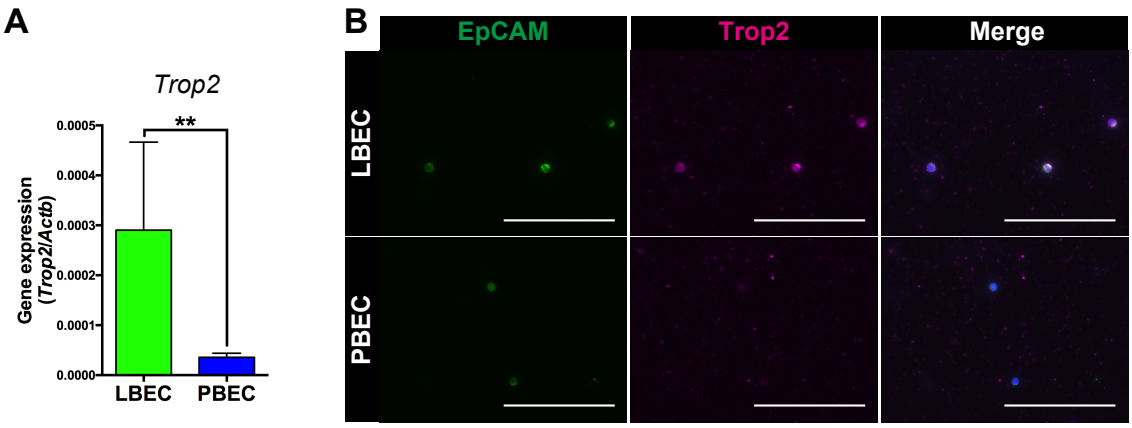

Figure 15. Expression analysis of Trop2 in isolated LBECs and PBECs.

(A) Gene expression analysis of *Trop2* in isolated LBECs and PBECs by qRT-PCR. Normalized values against *Actb* expression are shown as means ± SD (n = 6, $^{**}P < 0.01$). (B) Immunocytochemical analysis of freshly isolated LBECs and PBECs. After seeding of isolated LBECs and PBECs on slide glass, Trop2 expression of each cell fraction was confirmed by re-staining with anti-EpCAM and anti-Trop2 antibodies. Scale bars = 100 μm.

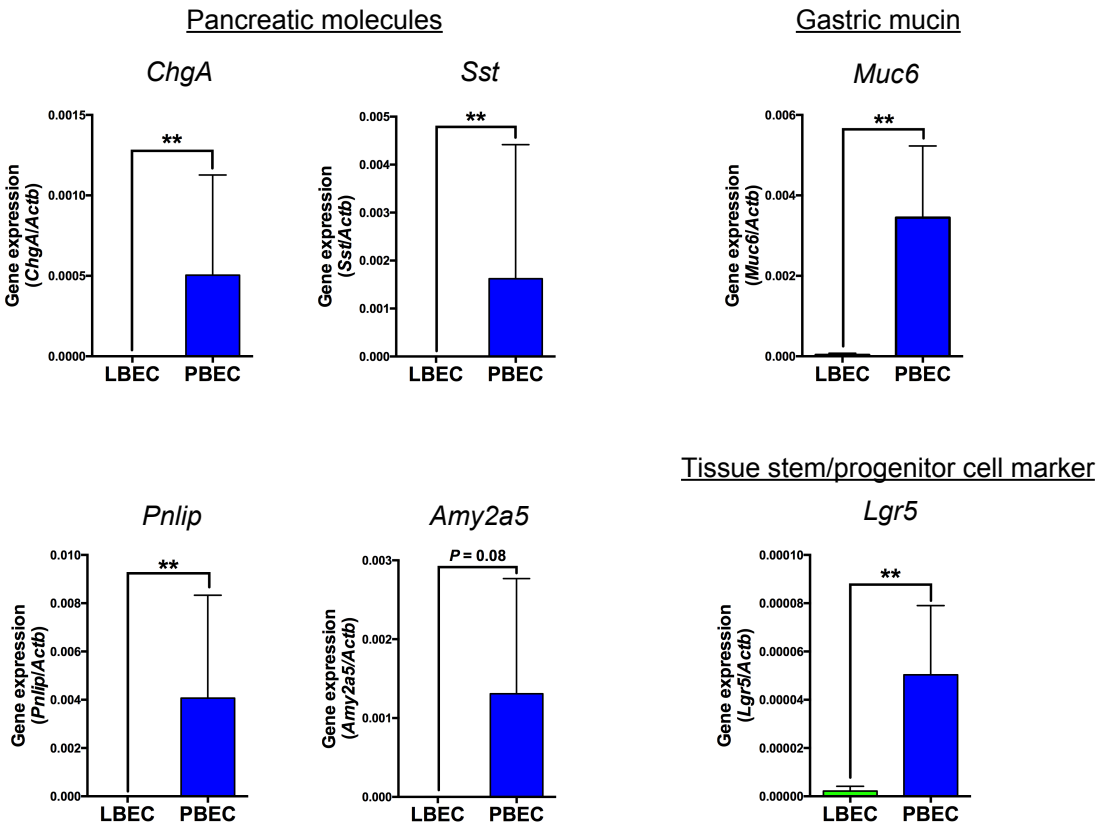

Figure 16. Characterization of isolated LBECs and PBECs by qRT-PCR.

Gene expression profiles of several PBG- and tissue stem/progenitor-related genes in LBECs and PBECs by qRT-PCR. Normalized values against *Actb* expression are shown as means ± SD (n = 6, $^{**}P < 0.01$).

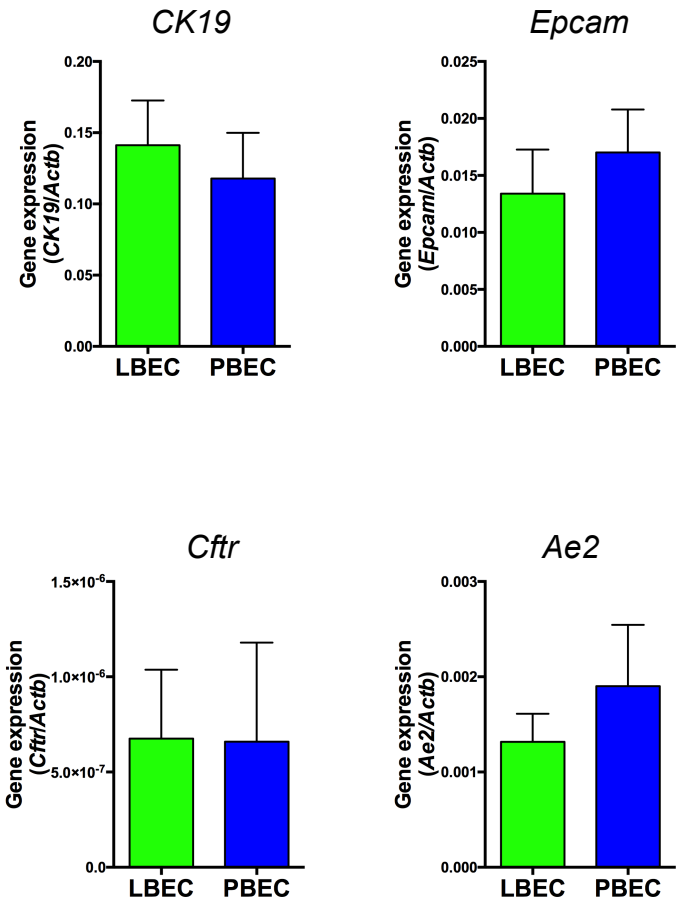

Figure 17. Analysis of several BEC markers in isolated LBECs and PBECs.

Gene expression analysis of several mature BEC markers in isolated LBECs and PBECs by qRT-PCR. Normalized values against *Actb* expression are shown as means ± SD (n = 6).

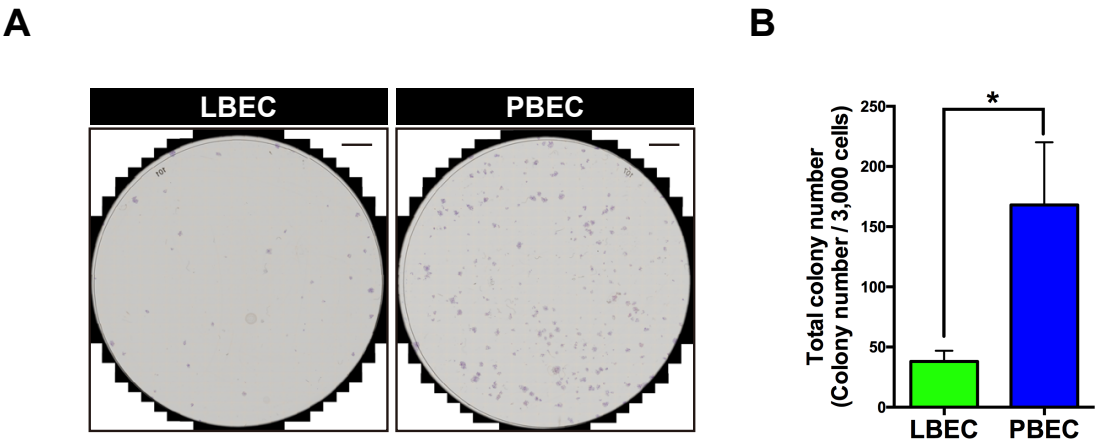

Figure 18. Characterization of isolated LBECs and PBECs by *in vitro* colony formation assay.

(A) Colony formation assay of LBECs and PBECs isolated from EHBD based on Trop2 expression. Representative images of colonies after Giemsa's staining are shown. Scale bars = 5 mm. (B) Measurement of colony number per 3,000 cells of isolated PBEC and LBEC. Values are shown as means ± SD (n = 3, **P* < 0.05).

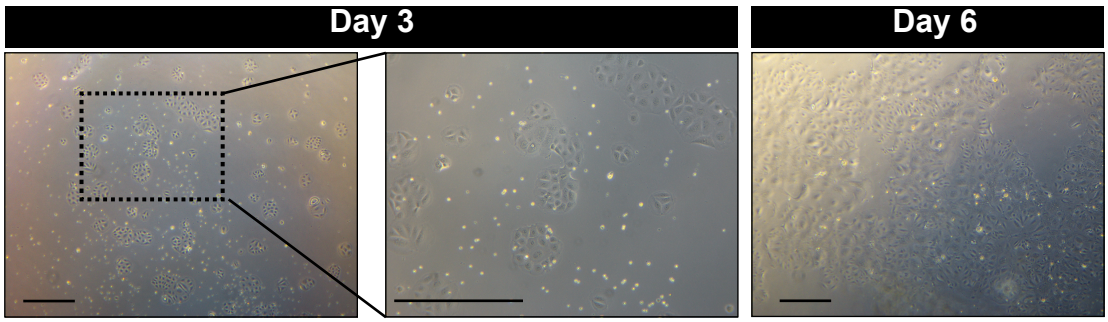

Figure 19. Cultured PBECs were expanded on the dish.

Expansion of the PBECs on the dish. Scale bars = 200 μm.

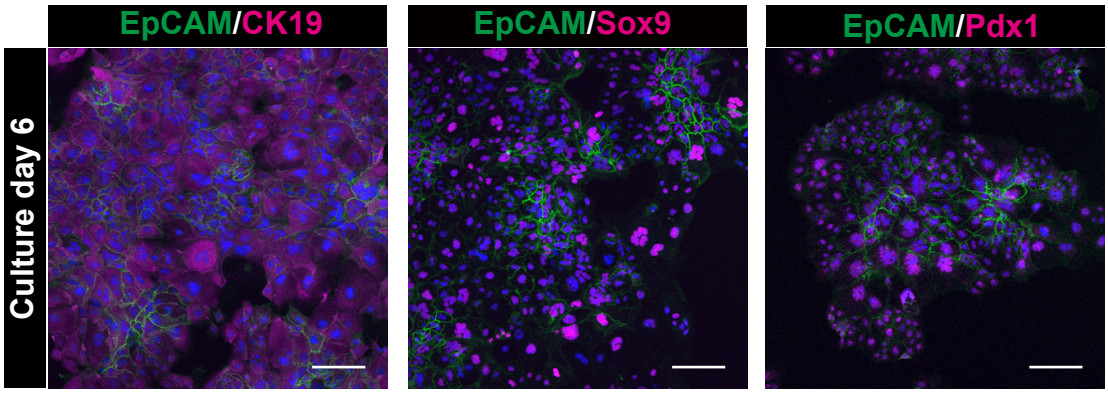

Figure 20. Characterization of the cultured PBECs by immunostaining.

Immunocytochemistry of cultured PBECs. The expressions of EpCAM, CK19, Sox9 and Pdx1 were maintained in cultured PBECs. Scale bars = 200 μm.

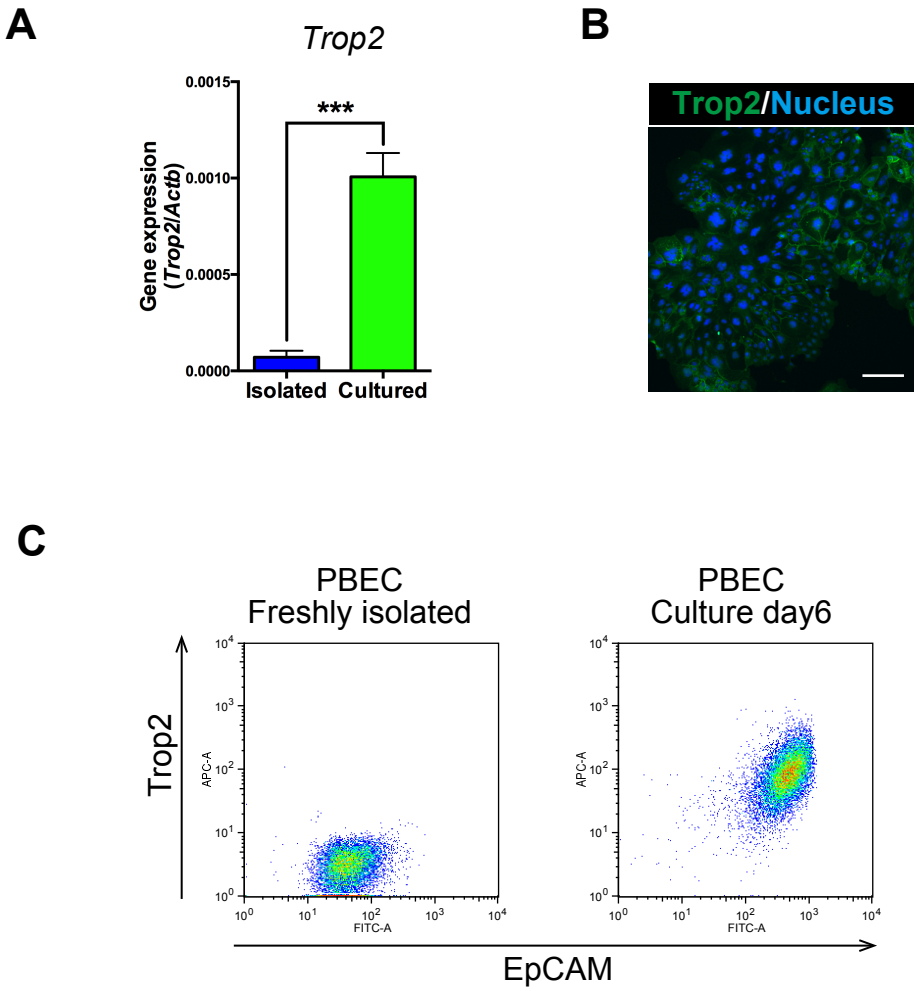

Figure 21. Expression analysis of Trop2 in cultured PBECs.

(A) Comparison of gene expressions of *Trop2* between freshly isolated and cultured PBECs by qRT-PCR. Normalized values against *Actb* expression are shown as means ± SD (n = 3-4, ***$P < 0.001$). (B) Expression of Trop2 in PBECs by immunostaining after expansion. Scale bar = 200 μm. (C) FCM analysis of freshly isolated and cultured PBECs with anti-EpCAM and anti-Trop2 antibodies.

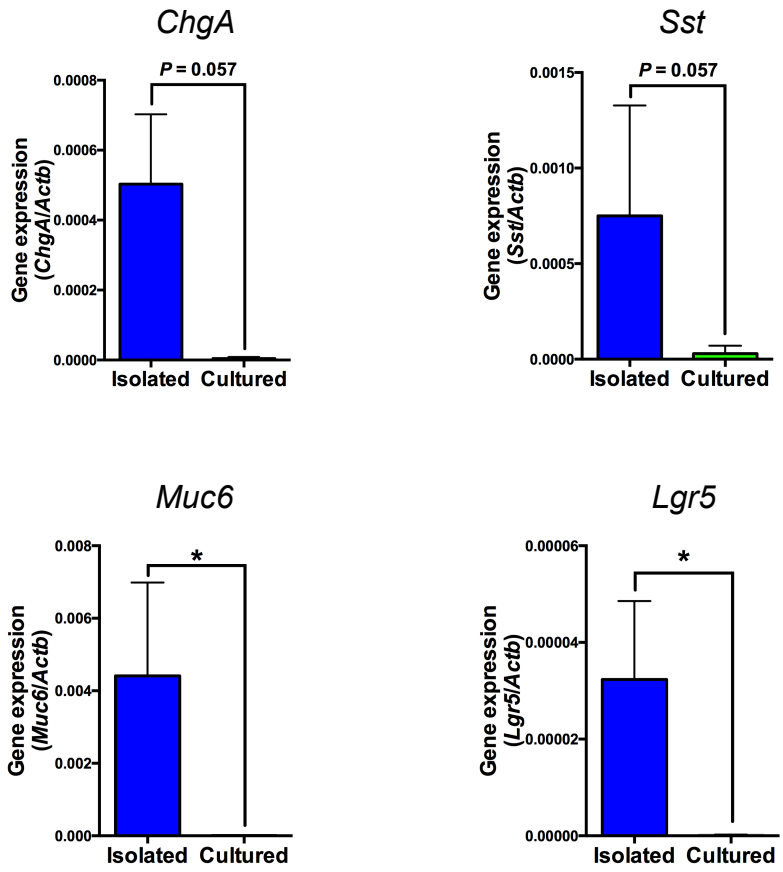

Figure 22. Expression analysis of PBG-related genes between freshly isolated and cultured PBECs.

Comparison of gene expressions of PBG-related genes (*ChgA, Sst, Muc6* and *Lgr5*) between freshly isolated and cultured PBECs by qRT-PCR. Normalized values against *Actb* expression are shown as means ± SD (n = 3-4, **P* < 0.05).

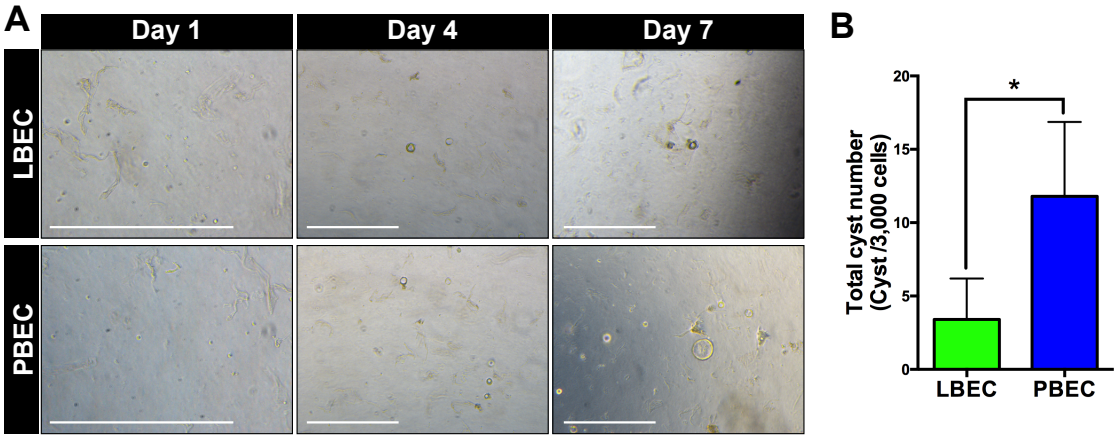

Figure 23. Cyst formation assay of isolated PBECs and LBECs.

(A) Morphology of LBECs and PBECs in 3D cyst culture condition. Scale bars = 200 μm. (B) The number of cysts per 3,000 cells is shown as means ± SD (n = 5, **P* < 0.05).

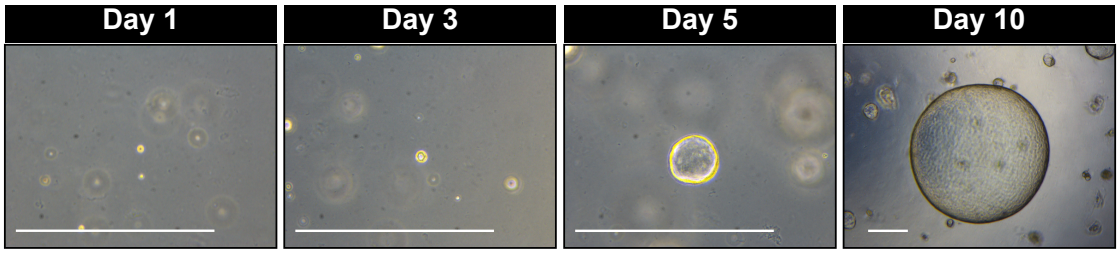

Figure 24. Growth of cystic-organoid derived from PBECs after 3D culture.

PBECs formed cystic-organoid. Scale bars = 200 μm.

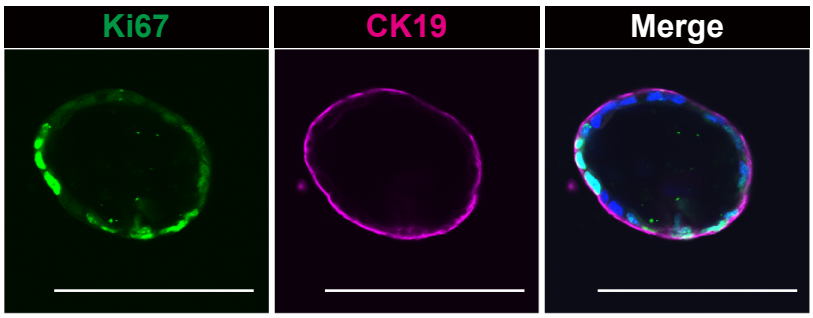

Figure 25. Analysis of the cell proliferation in cystic-organoid.

Immunostaining of cystic-organoid with anti-CK19 and Ki67 antibodies. Scale bars = 200 μm.

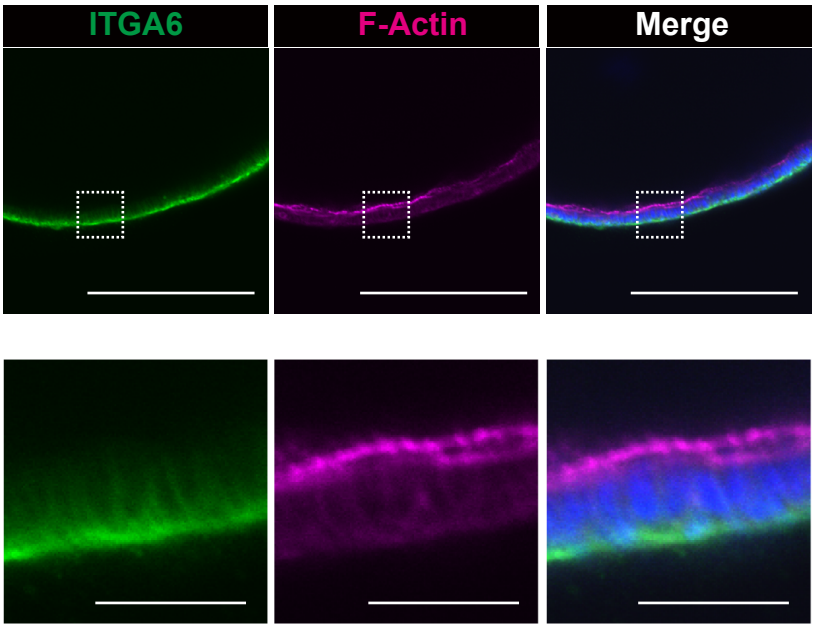

Figure 26. Analysis of the epithelial polarity markers localization in cystic-organoid.

Immunostaining of cystic-organoid stained with anti-ITGA6 antibody and phalloidin. The cystic-organoid exhibited cyst-like structure with normal epithelial polarity. Scale bars = 200 μm (upper panel) and 30 μm (lower panel). Dashed boxes indicates magnified region.

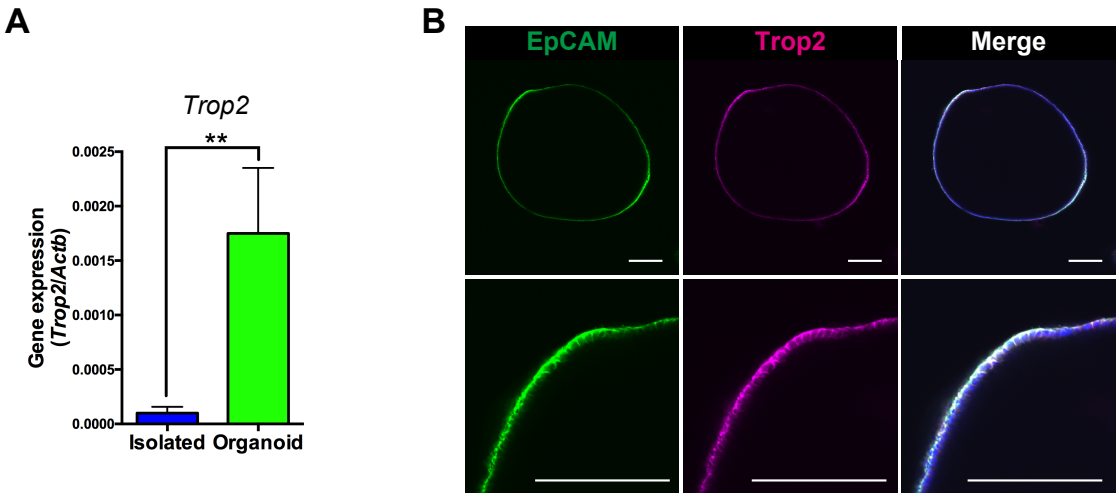

Figure 27. Expression analysis of Trop2 in cystic-organoid.

(A) Comparison of gene expressions of *Trop2* between freshly isolated and organoid-forming PBECs by qRT-PCR. Normalized values against *Actb* expression are shown as means ± SD (n = 4-6, ***P* < 0.01). (B) Immunostaining of PBEC-derived cystic-organoid with anti-EpCAM and anti-Trop2 antibodies. Scale bars = 200 μm.

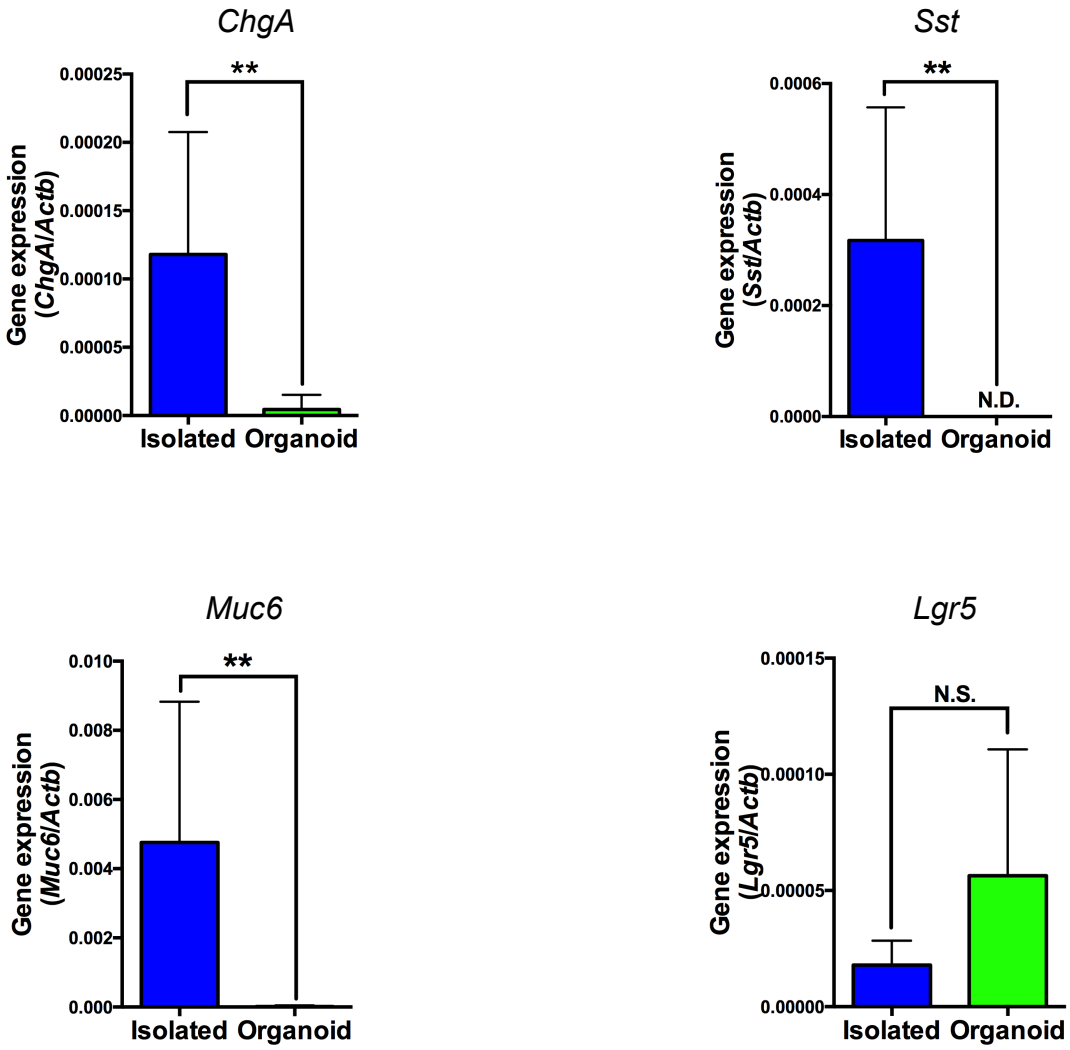

Figure 28. Expression analysis of PBG-related genes between freshly isolated and organoid-forming PBECs.

Comparison of gene expressions of PBG-related genes (*ChgA*, *Sst*, *Muc6* and *Lgr5*) between freshly isolated and organoid-forming PBECs by qRT-PCR. Normalized values against *Actb* expression are shown as means ± SD (n = 4-6, ***P* <0 .01). N.D.: not detected, N.S.: not significant.

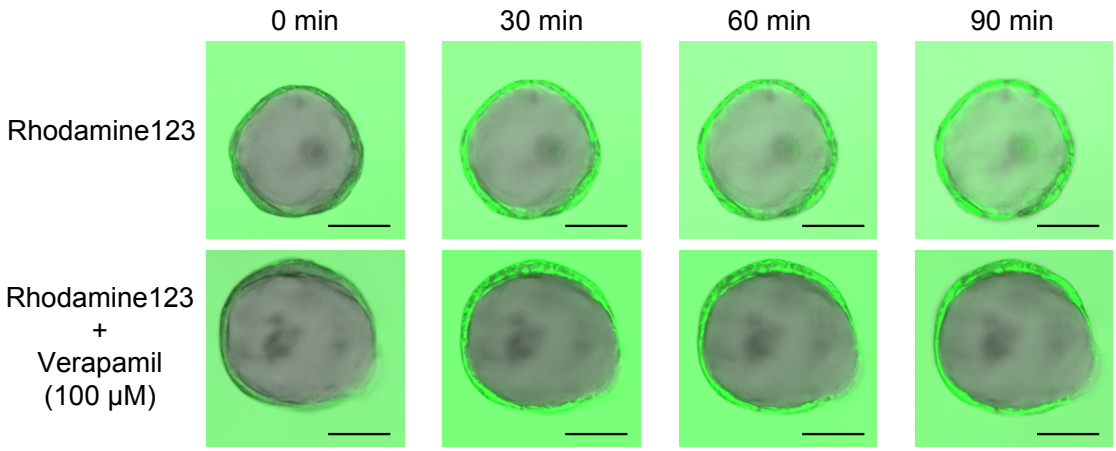

Figure 29. Rhodamine 123 incorporation assay for cystic-organoid.

Confocal microscopic images of Rhodamine123 incorporation in cystic-organoid. Rhodamine123 was gradually accumulated in the luminal space of cystic-organoid in a time-dependent manner (upper panel). Rhodamine123 accumulation was blocked by pretreatment of cystic-organoid with verapamil (lower panel). Scale bars = 100 μm.

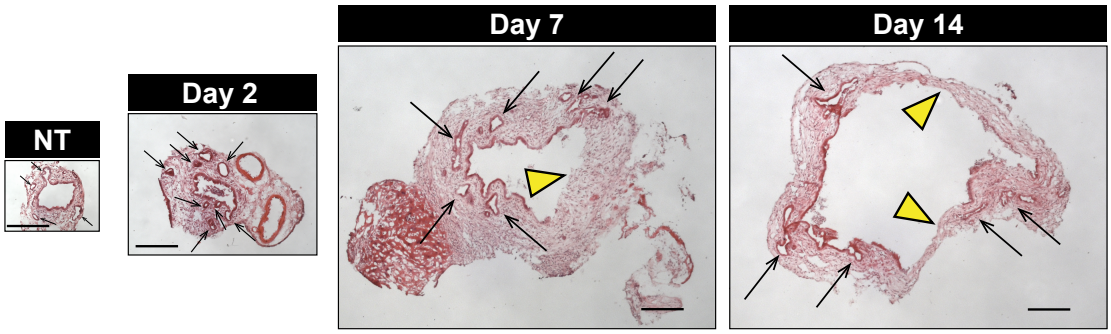

Figure 30. Histological analysis of EHBD after BDL.

H&E staining of non-treated (NT) and injured mouse EHBD. The detachment of damaged luminal epithelium is denoted with yellow arrowheads. Scale bars = 200 μm. Arrows indicate PBGs.

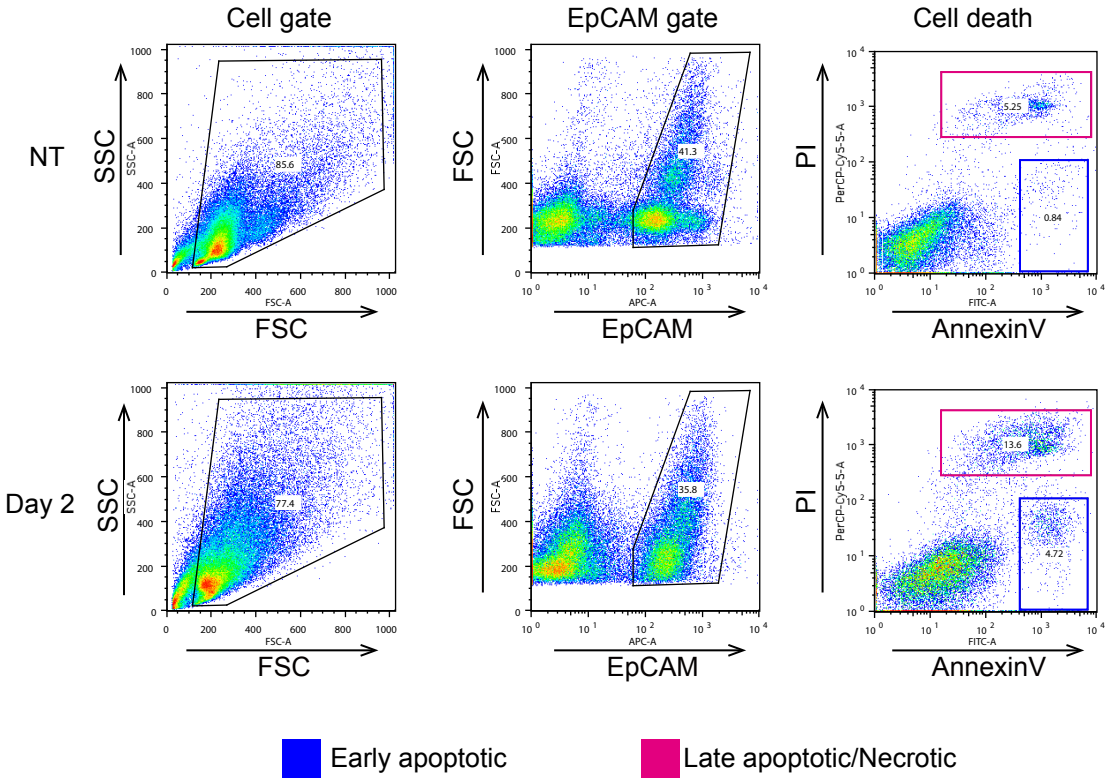

Figure 31. FCM analysis for the evaluation of cell death in EHBD.

Non-treated (NT) and BDL-treated adult mouse EHBD cells were stained with anti-EpCAM antibody, Annexin V and propidium iodide (PI). After 2 days of BDL, apoptotic and necrotic BECs increased remarkably, compared to NT BECs. FSC: forward scatter, SSC: side scatter.

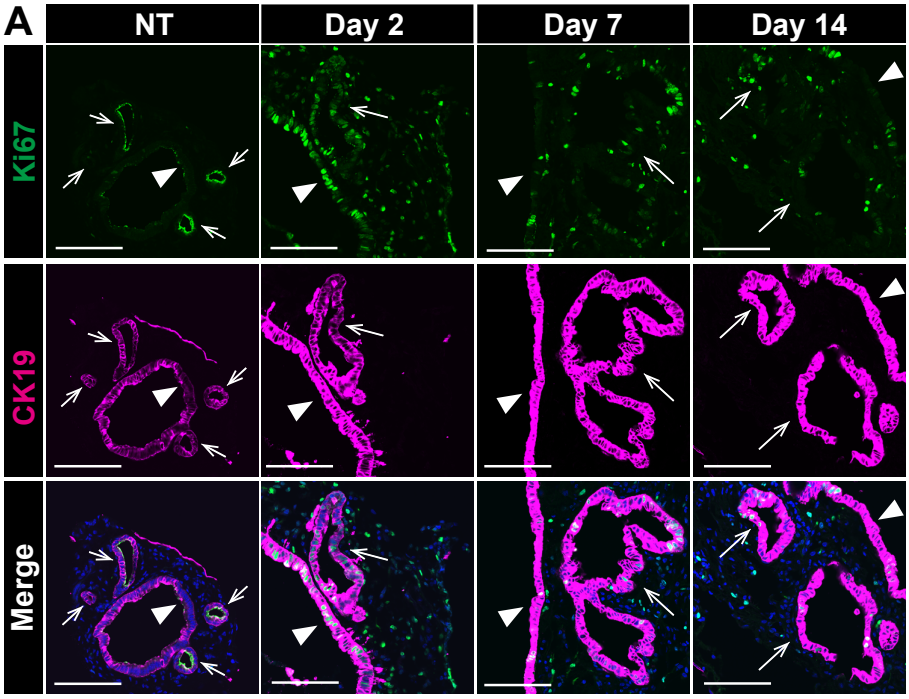
A
NT
Day 2
Day 7
Day 14
Ki67
CK19
Merge

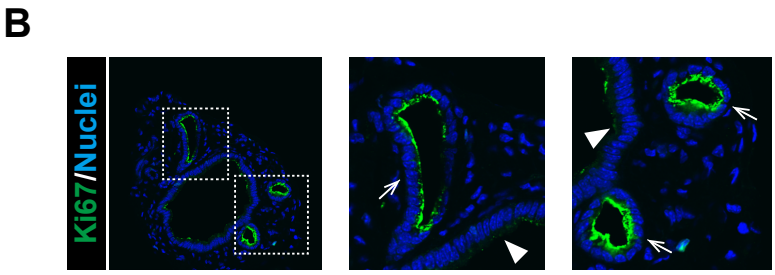
B
Ki67/Nuclei

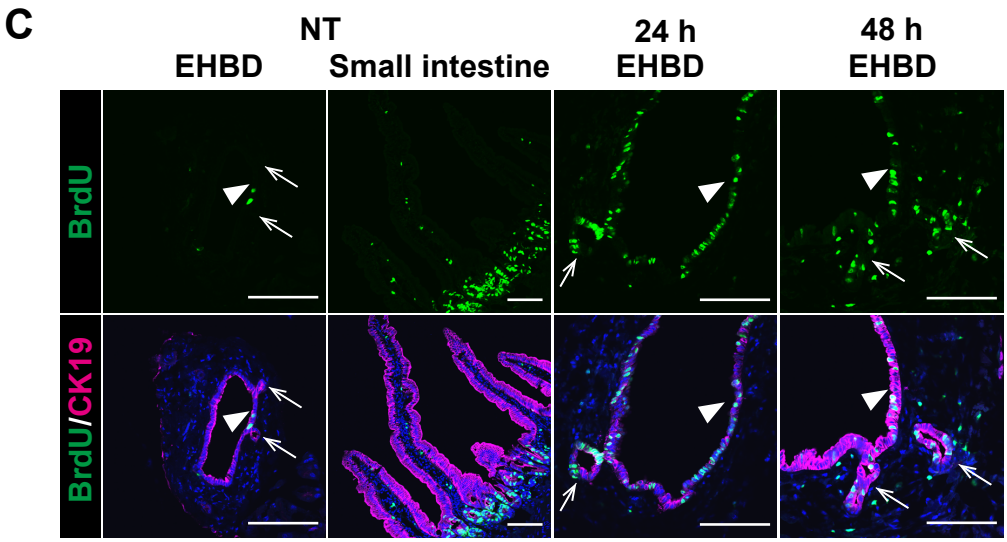
C
NT
EHBD
Small intestine
24 h
EHBD
48 h
EHBD
BrdU
BrdU/CK19

Figure 32. Analysis of cell proliferation in injured EHBD.

Analysis of cell proliferation status in injured EHBD. (A) Transverse sections of EHBD were stained with anti-Ki67 and anti-CK19 antibodies. (B) Magnified images of non-treated EHBD sample shown in panel A. Dashed boxes indicate magnified region. (C) BrdU incorporation assay of EHBD. Transverse sections of EHBD in non-treated or injured mice (24h and 48h) were stained with anti-BrdU and anti-CK19 antibodies. Small intestine of non-treated mouse was used as a positive control. Scale bars = 100 μm. PBGs are denoted with arrows, and the luminal epithelia are denoted with arrowheads. NT: non-treated.

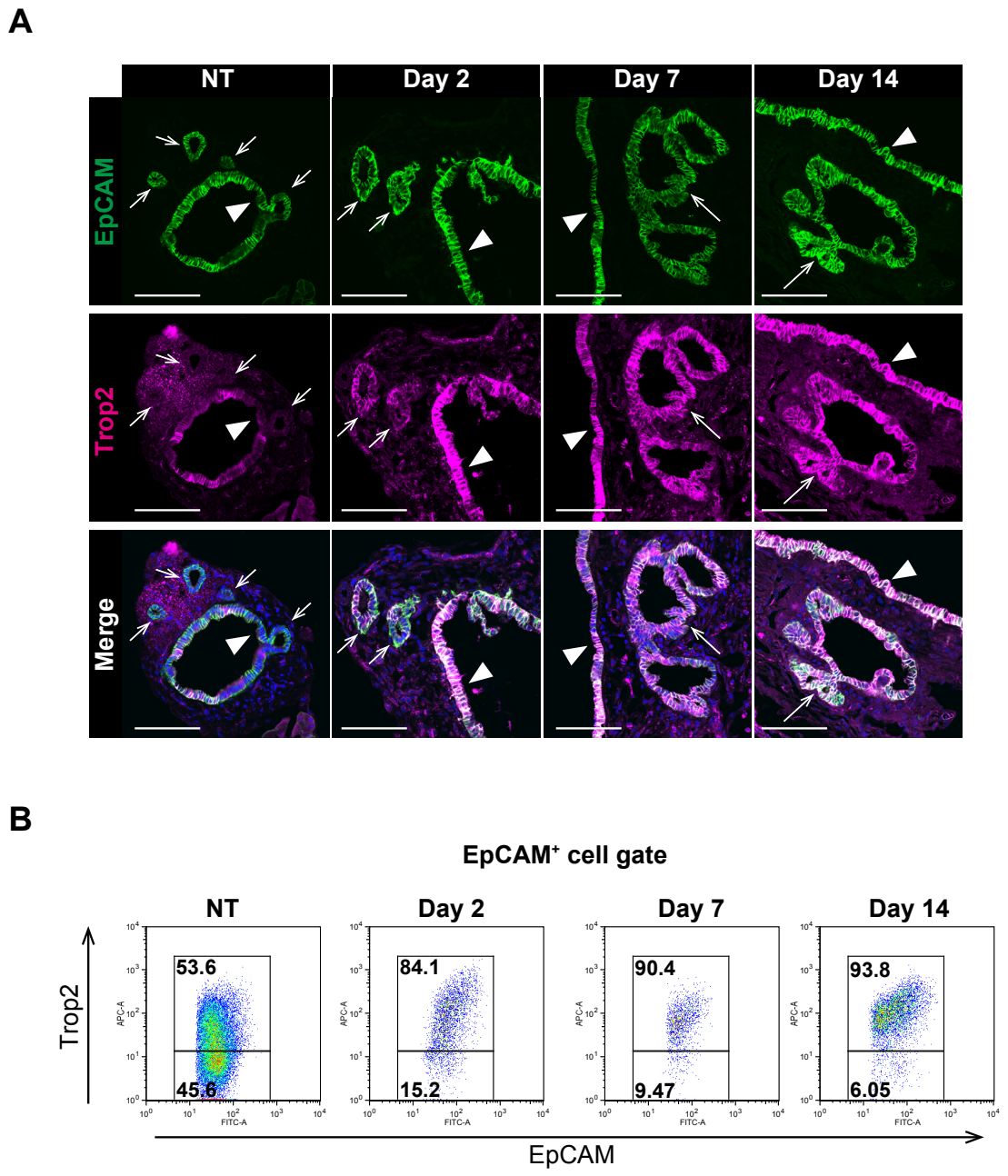

Figure 33. Expression analysis of Trop2 after BDL.

(A) Expression analysis of Trop2 in non-treated (NT) and injured EHBD by immunostaining. Transverse sections of EHBD were stained with anti-EpCAM and anti-Trop2 antibodies. Trop2 expression was induced in PBGs upon biliary injury. PBGs are denoted with arrows, and the luminal epithelia are denoted with arrowheads. Scale bars = 100 μm. (B) FCM analysis of NT and injured EHBD with anti-EpCAM and Trop2 antibodies.

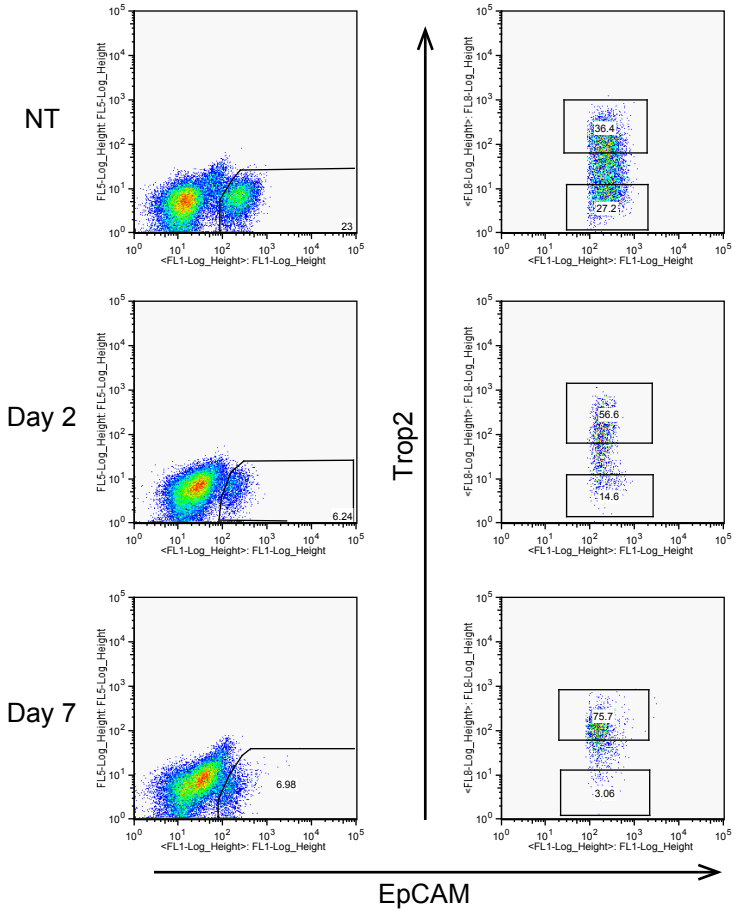

Figure 34. FACS analysis of EHBD cells after BDL.

The indicated gate was set for isolation of $Trop2^{+}$ and $Trop2^{-}$ BECs fractions for colony formation assay. NT: non-treated.

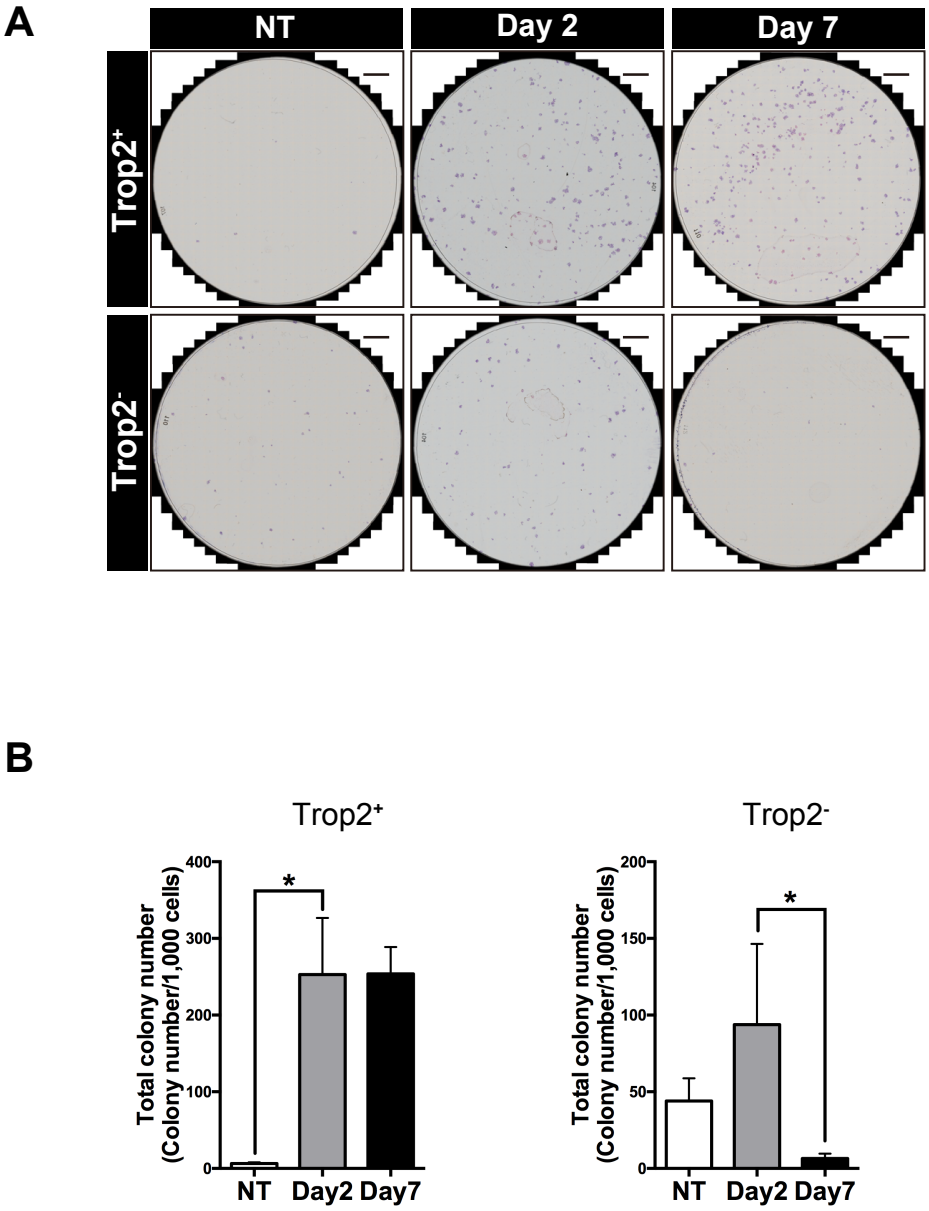

Figure 35. Colony formation assay of isolated Trop2$^+$ and Trop2$^-$ BECs after BDL.

(A) Colony formation assay of Trop2$^+$ and Trop2$^-$ BECs isolated from non-treated (NT) and injured EHBD. Representative images of colonies after Giemsa's staining are shown. Scale bars = 5 mm. (B) Colony formation assay of Trop2$^+$ and Trop2$^-$ BECs isolated from NT and injured EHBD. The colony number per 1,000 cells is shown as means ± SD (n = 3-5, *P < 0.05).

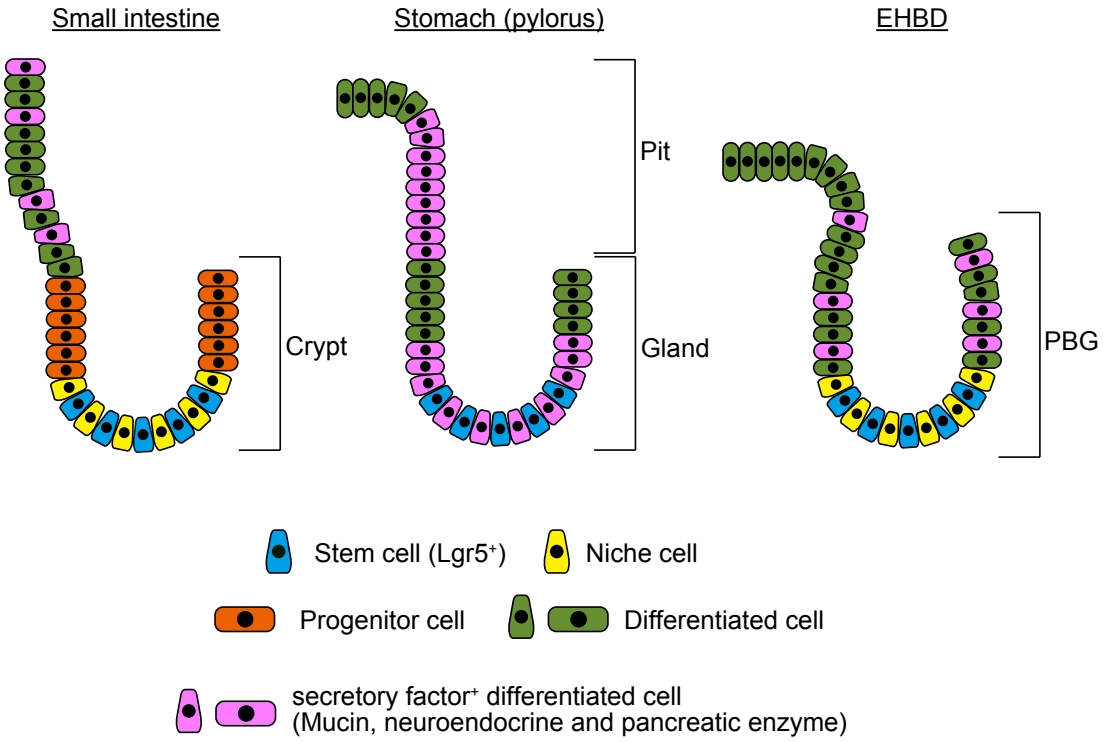

Figure 36. Schematic diagram of gastrointestinal crypts and the hypothesis of PBG structure.

$Lgr5^+$ tissue stem cells are located in bottom of crypt and gland. Gland of stomach contains mucus producing cell. PBGs showed similar gene expression profile and regeneration to these organs. I hypothesis that PBGs form similar heterogeneous hierarchical structure to these organs.

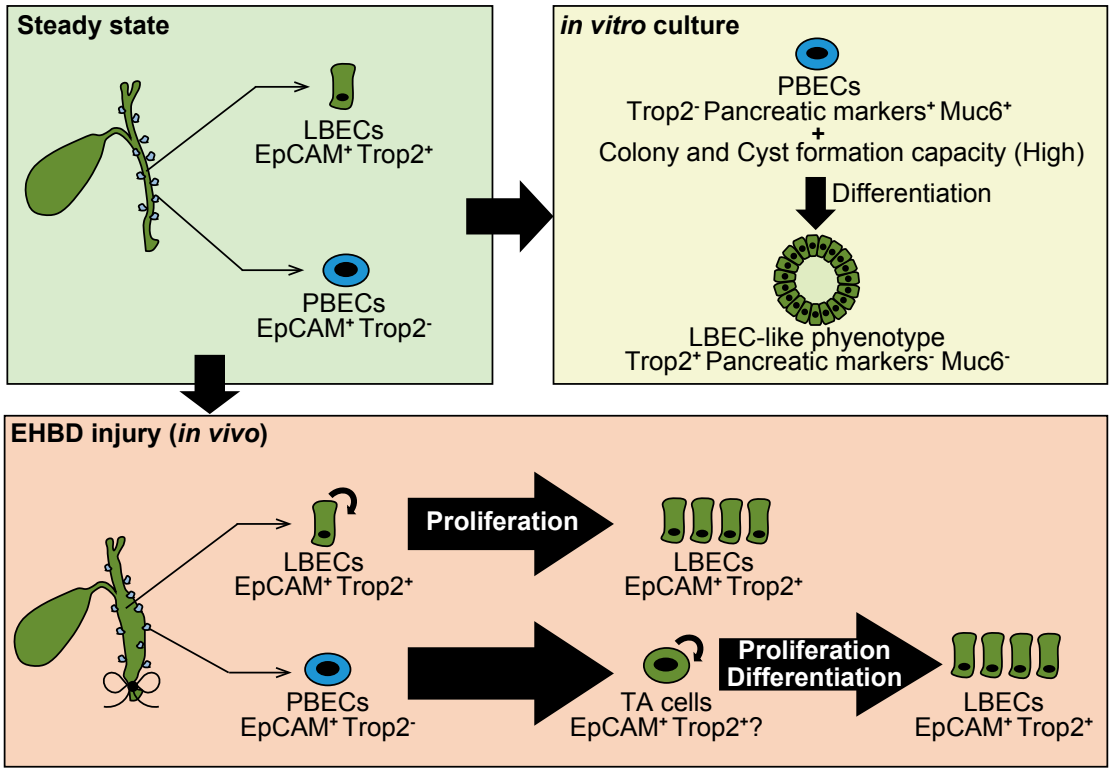

Figure 37. Schematic summary of the present study.

(Upper left panel) The characteristics of the LBECs and PBECs at steady state. The differential expression profiles of Trop2 in EHBD makes it possible to discriminate between LBECs and PBECs by FACS. (Upper right panel) The isolated PBECs show higher colony formation capacity than LBECs *in vitro*. The expanded PBECs have a potential for forming cysts composed of LBEC-like $Trop2^{+}$ cells with luminal epithelial polarity in the 3D organoid culture. (Lower panel) Model of biliary regeneration by PBECs after injury. By BDL, Trop2 expression is rapidly induced in PBGs *in vivo* and PBECs proliferated, giving rise to transit-amplifying (TA) cells for the luminal epithelium regeneration.

Table 1. Review of the LPC induction models and diseases

Spiecies	Model or disease	References
Human	Hepatitis C	Lowes *et al*., 1999; Sun *et al*., 2006
	Hepatitis B	Sun *et al*., 2006
	Alcoholic liver disease	Lowes *et al*., 1999
	Genetic hemochromatosis	Lowes *et al*., 1999
	Acute necrotising hepatitis	Spee *et al*., 2010
	Primary biliary cirrhosis	Spee *et al*., 2010
	Extrahepatic biliary atresia	Baumann *et al*., 1999
	Fulminant hepatic failure	Baumann *et al*., 1999
	NAFLD	Nobili *et al*., 2012
	NASH	Richardson *et al*., 2007
Mouse	Dipin+PHx	Factor *et al*., 1994
	DDC	Preisegger *et al*., 1999
	Phenobarbital+Cocaine	Rosenberg *et al*., 2000
	Allyl alcohol	Lee *et al*., 1996
	CDE	Knight *et al*., 2000
	Modified CDE	Akhurst *et al*., 2001
	BDL	Sackett *et al*., 2009
	CCl4	Gleiberman *et al*., 2005
	High-fat diet+ethanol	Jung *et al*., 2008
	Alb-Cre/DDB1$^{flox/flox}$	Endo *et al*., 2012
	Ah-Cre/Mdm2$^{flox/flox}$	Lu *et al*., 2015
Rat	2-AAF	Farber 1956: Teebor *et al*., 1971
	DEN	Schwarze *et al*., 1984
	Solt-Farber model (2-AAF+DEN+PHx)	Solt *et al*., 1977
	Modified Solt-Farber model (2-AAF+PHx)	Evarts *et al*., 1987 and 1990
	2-AAF+CCl4	Petersen *et al*., 1998
	3'-Me-DAB	Farber. 1956
	Ethione	Farber. 1956
	Allyl alcohol	Yavorkovsky *et al*., 1995
	CDE	Shinozuka *et al*., 1978
	D-Galactosamine	Lesch *et al*., 1970; Lemire *et al*., 1991; Dabeva *et al*., 1993
	Lasiocarpine+PHx	Laconi *et al*., 1995
	Wilson's disease model (Long-Evans Cinnamon rat)	Yasui *et al*., 1997
	Retrosine+PHx	Laconi *et al*., 1998; Gordon *et al*., 2000
Zebrafish	Depletion of the hepatocyte (Metronidazole+fabp10a:CFP-NTR)	Choi *et al*., 2014

Tabel 2. List of LPC marker genes

Spiecies	Maker gene	References
Human	CK19	Roskams *et al*., 1996
	CK7	Roskams *et al*., 1996
	EpCAM	Schmelzer *et al* .,2007
	CD34	Crosby *et al*., 2001
	c-Kit	Baumann *et al*., 1999; Crosby *et al*., 2001
	OV-6	Roskams *et al*., 1996; Crosby *et al*., 1998
	ALDH	Dolle´ *et al*., 2012
Mouse	CK19	Wang *et al*., 2003
	CD133	Rountree *et al*., 2007; Suzuki *et al*., 2008; Kamiya *et al*., 2009
	EpCAM	Okabe *et al*., 2009
	Trop2	Okabe *et al*., 2009
	CD24	Qiu *et al*., 2011
	MIC1-1C3	Dorrell *et al*., 2011
	Lgr5	Huch *et al*., 2013a
	A6	Engelhardt *et al*., 1990
	Sox9	Furuyama *et al*., 2011; Dorrell *et al*., 2011
	Alb	Dumble *et al*., 2002
	c-Kit	Wang *et al*., 2003
	Sca-1	Petersen *et al*., 2003
	Opn	Español-Suñer *et al*., 2012
	HNF1β	Rodrigo-Torres *et al*., 2014; Jörs *et al*., 2015
	Foxl1	Sackett *et al*., 2009; Shin *et al*., 2011
Rat	CK19	Tatematsu *et al*., 1985
	CK7	Paku *et al*., 2005
	CD133	Yovchev *et al*., 2007
	EpCAM	Yovchev *et al*., 2007
	CD24	Yovchev *et al*., 2007
	CD34	Omori *et al*., 1997
	CD44	Yovchev *et al*., 2007
	Alb	Yaswen *et al*., 1984
	Afp	Yaswen *et al*., 1984; Lemire *et al*., 1991
	c-Kit	Fujio *et al*., 1994
	Dlk1	Jensen *et al*., 2004
	OV-6	Dunsford *et al*., 1989
	Thy1	Petersen *et al*., 1998
	GGT	Evarts *et al*., 1989

Table 3. Review of EHBD injury models and diseases

Spiecies	Models or diseases	References
Human	Hepatolithiasis	Kurumaya *et al*., 1989
	Cholangitis/Cholecystitis	Sutton *et al*., 2012
	Ischaemic type biliary lesions	Sutton *et al*., 2012
	Primary sclerosing cholangitis	Carpino *et al*., 2015
	Type2 diabetes	Carpino *et al*., 2016
Mouse	BDL	Irie *et al*., 2007; Dipaola *et al*., 2013
	Rhesus rotavirus infection	Shivakuma *et al*., 2004; Dipaola *et al*., 2013; Li *et al*., 2014
	KTC-CK19Cre^{ERT} (Kras, TGFβR2, and E-Cadherin conditional KO)	Nakagawa *et al*., 2017
	STZ	Carpino *et al*., 2016
Rat	BDL	Cohen *et al*., 1964

Table 4. Antibodies used in this study

Protein	Host animal	Conjugate	Company/Source	Experiment	Dilution
CK19	Rabbit	-	Tanimizu *et al*., 2003	IHC, ICC	1:1000
Sox9	Rabbit	-	Merck Millipore (AB5535; Burlington, MA)	IHC, ICC	1:1000
EpCAM	Rat	-	BD Biosciences (552370; Franklin Lakes, NJ)	IHC, ICC	1:100
EpCAM	Rat	FITC and Biotin	Okabe *et al*., 2009	FCM	1:50 and 1:100
Trop2	Goat	Biotin	R&D systems (BAF1122; Minneapolis, MN)	IHC, ICC, FCM	1:100
ITGA6	Rat	-	BD Biosciences (555734)	ICC	1:200
Opn	Goat	-	R&D systems (AF808)	IHC	1:200
Pdx1	Guinea pig	-	abcam (ab47308; Cambridge, MA)	IHC, ICC	1:200
Cftr	Rabbit	-	abcam (ab59394)	IHC	1:50
Ki67	Rat	-	eBioscience (14-5698-82; San Diego, CA)	IHC, ICC	1:200
BrdU	Rat	-	abcam (ab6326)	IHC	1:100
Phalloidin	-	Alexa Fluor 555	Thermo Fisher Scientific (A34055; Waltham, MA)	ICC	1:200
FcR blocker	Purified anti-CD16/CD32 antibody		Hybridoma 2.4G2 clone	FCM	1:100
			Biolegend (101302; San Diego, CA)	FCM	1:500

Table 5. Medium composition used for isolated LBEC and PBEC culture

Reagents	Company/Source	Final concentration
Williams' Medium E	Thermo Fisher Scientific (Waltham, MA)	-
BSA (Fatty acid free)	Sigma-Aldrich (St. Louis, MO)	0.1%
L-glutamine	Thermo Fisher Scientific	2 mM
Glucose	Wako Pure Chemical Industries (Osaka, Japan)	14 mM
HEPES	Thermo Fisher Scientific	20 mM
Sodium pyruvate	Thermo Fisher Scientific	1 mM
Sodium hydrogen carbonate	Wako Pure Chemical Industries	0.15%
Nicotinamide	Sigma-Aldrich	10 mM
Ascorbic acid	Sigma-Aldrich	0.2 mM
B27	Thermo Fisher Scientific	2%
ITS-X	Thermo Fisher Scientific	1%
Recombinant mouse EGF	PeproTech (London, UK)	10 ng/ml
Recombinant human HGF	PeproTech	10 ng/ml
Dexamethasone	Wako Pure Chemical Industries	0.1 μM
Gentamicin	Wako Pure Chemical Industries	50 μg/ml

Table 6. Medium composition used for the 3D organoid culture

Reagents	Company/Source	Final concentration
Advanced DMEM/F12	Thermo Fisher Scientific (Waltham, MA)	-
GlutaMAX	Thermo Fisher Scientific	1%
HEPES	Thermo Fisher Scientific	10 mM
Nicotinamide	Sigma-Aldrich (St. Louis, MO)	10 mM
B27	Thermo Fisher Scientific	2%
N-Acetyl-L-cysteine	Sigma-Aldrich	1.25 mM
Gastrine	Sigma-Aldrich	10 nM
Recombinatn Mouse EGF	PeproTech (London, UK)	50 ng/ml
Recombinant Human Rspondin-1	PeproTech	500 ng/ml
Recombinant Human FGF10	PeproTech	100 ng/ml
Recombinant Mouse Noggin	PeproTech	100 ng/ml
Y27632	Sigma-Aldrich	10 nM
Penicillin-Streptomycin	Thermo Fisher Scientific	2%

Table 7. Primers and probes used for qRT-PCR

Gene	Probe	Orientation	Primer sequence
Ae2	#1	Forward	5' ATGTGGCCTCACTGTCCTTC 3'
		Reverse	5' GCTGATCGAGGTCTAAGAGCA 3'
Amy2a5	#7	Forward	5' AGTGGAATGGCGAGAAGATG 3'
		Reverse	5' CTGTCAGAAGGCACCAAACC 3'
Cftr	#51	Forward	5' CAGCAGCTCAAACAACTGGA 3'
		Reverse	5' TGTCACAAGGTGGGTGAAAA 3'
ChgA	#58	Forward	5' AGGCTACAAAGCGATCCAGA 3'
		Reverse	5' CGGAAGCCTCTGTCTTTCC 3'
CK19	#97	Forward	5' AGTCCCAGCTCAGCATGAA 3'
		Reverse	5' TAACGGGCCTCCGTCTCT 3'
Epcam	#52	Forward	5' AGAATACTGTCATTTGCTCCAAACT 3'
		Reverse	5' GTTCTGGATCGCCCCTTC 3'
Lgr5	#38	Forward	5' CTACCCGCCAGTCTCCTACA 3'
		Reverse	5' AAAGCATTTCCAGCAAGACG 3'
Muc6	#89	Forward	5' GGATGTCTACCAGCCAAGGT 3'
		Reverse	5' AACGATGTGGACTGATGCTG 3'
Pdx1	#51	Forward	5' GAAATCCACCAAAGCTCACG 3'
		Reverse	5' CGGGTTCCGCTGTGTAAG 3'
Pnlip	#32	Forward	5' CTGTGGACATTTGCAGTGCT 3'
		Reverse	5' TGAAGCAGCCGAGTTTGTC 3'
Sst	#53	Forward	5' CCCAGACTCCGTCAGTTTCT 3'
		Reverse	5' GGGCATCATTCTCTGTCTGG 3'
Trop2	#17	Forward	5' CGGGCAAATACAAAAAGGTG 3'
		Reverse	5' ACAAGCTAGGTTCGCTTCTCA 3'

Table 8. List of top30 and gastrointestinal-related genes

Gene symbol	Gene name	log_2 (PBEC/LBEC)
Chga	Chromogranin A	10.39
Sst	Somatostatin	10.12
Pcdh20	Protocadherin 20	8.84
Chgb	Chromogranin B	8.26
Iapp	Islet amyloid polypeptide	8.10
Hck	Hemopoietic cell kinase, transcript variant 1	8.00
Rgs13	Regulator of G-protein signaling 13	7.66
Ghrl	Ghrelin, transcript variant 1	7.55
Ppy	Pancreatic polypeptide	7.46
Cpb1	Carboxypeptidase B1	7.05
Pnlip	Pancreatic lipase	6.99
Strip2	Striatin interacting protein 2, transcript variant 1	6.96
Amy2a5	Amylase 2a5	6.87
Fyb	FYN binding protein	6.61
Pcolce2	Procollagen C-endopeptidase enhancer 2	6.41
Rbp4	Retinol binding protein 4, plasma, transcript variant 2	6.40
Scg2	Secretogranin II	6.32
Hmx2	H6 homeobox 2	6.30
Prss2	Protease, serine 2	6.28
Cyp4a30b	Cytochrome P450, family 4, subfamily a, polypeptide 30b	6.26
Dgki	Diacylglycerol kinase, iota	6.24
Sv2c	Synaptic vesicle glycoprotein 2c	6.18
Alox5	Arachidonate 5-lipoxygenase	6.10
Cpe	Carboxypeptidase E	6.05
Lgr5	Leucine rich repeat containing G protein coupled receptor 5	6.04
Try4	Trypsin 4	6.03
Gnat3	Guanine nucleotide binding protein, alpha transducing 3	5.97
Nrg4	Neuregulin 4	5.93
St18	Suppression of tumorigenicity 18, transcript variant 3	5.91
Trop2	Tumor associated calcium signal transducer 2	-2.88
Muc6	Mucin 6, gastric	5.43
Dclk1	Doublecortin-like kinase 1	4.10

Table 9. List of tissue stem/progenitor cell- and pluripotent-related genes

Gene symbol	Gene name	log_2 (PBEC/LBEC)
Dner	Delta/notch-like EGF-related receptor	5.53
Gp2	Glycoprotein 2	5.33
Olfm4	Olfactomedin 4	2.81
Ascl2	Achaete-scute complex homolog 2	2.45
Nanog	Nanog, homeobox	-0.03
Oct4	Octamer-binding transcription factor	-0.08
Sox2	Sex determining region Y-box 2	-0.52

Green: Tissue stem/progenitor cell-related genes

Yellow: Pluripotent-related genes

References

1. Alastair D. Burt, Linda D. Ferrell and Stefan G Hubscher. MacSween's Pathology of the Liver, 6th Edition. CHURCHILL LIVINGSTONE (UK). 2012.

2. Orkin SH, Zon LI. Hematopoiesis: an evolving paradigm for stem cell biology. Cell. 2008;132:631-644.

3. Poisson J, Lemoinne S, Boulanger C, Durand F, Moreau R, Valla D, Rautou PE. Liver sinusoidal endothelial cells: Physiology and role in liver diseases. J Hepatol. 2017;66:212-227.

4. Bilzer M, Roggel F, Gerbes AL. Role of Kupffer cells in host defense and liver disease. Liver Int. 2006;26:1175-1186.

5. Tsuchida T, Friedman SL. Mechanisms of hepatic stellate cell activation. Nat Rev Gastroenterol Hepatol. 2017;14:397-411.

6. Boyer JL. Bile formation and secretion. Compr Physiol. 2013;3:1035-1078.

7. Saxena R, Theise N. Canals of Hering: recent insights and current knowledge. Semin Liver Dis. 2004;24:43-48.

8. Marzioni M, Glaser SS, Francis H, Phinizy JL, LeSage G, Alpini G. Functional heterogeneity of cholangiocytes. Semin Liver Dis. 2002;22:227-240.

9. Kaneko K, Kamimoto K, Miyajima A, Itoh T. Adaptive remodeling of the biliary architecture underlies liver homeostasis. Hepatology. 2015;61:2056-2066.

10. Ishida F, Terada T, Nakanuma Y. Histologic and scanning electron microscopic observations of intrahepatic peribiliary glands in normal human livers. Lab Invest. 1989;60:260–265.

11. Nakanuma Y, Katayanagi K, Terada T, Saito K. Intrahepatic peribiliary glands of humans. I. Anatomy, development and presumed functions. J Gastroenterol Hepatol. 1994;9:75-79.

12. Nakanuma Y, Hoso M, Sanzen T, Sasaki M. Microstructure and development of the normal and pathologic biliary tract in humans, including blood supply. Microsc Res Tech. 1997;38:552-570.

13. Terada T, Kida T, Nakanuma Y. Extrahepatic peribiliary glands express alpha-amylase isozymes, trypsin and pancreatic lipase: an immunohistochemical analysis. Hepatology. 1993;18:803-808.

14. Dipaola F, Shivakumar P, Pfister J, Walters S, Sabla G, Bezerra JA. Identification of intramural epithelial networks linked to peribiliary glands that express progenitor cell markers and proliferate after injury in mice. Hepatology. 2013;58:1486-1496.

15. Zong Y, Stanger BZ. Molecular mechanisms of bile duct development. Int J Biochem Cell Biol. 2011;43:257-264.

16. Spence JR, Lange AW, Lin SC, Kaestner KH, Lowy AM, Kim I, Whitsett JA, Wells JM. Sox17 regulates organ lineage segregation of ventral foregut progenitor cells. Dev Cell. 2009;17:62-74.

17. Bort R, Signore M, Tremblay K, Martinez Barbera JP, Zaret KS. Hex homeobox gene controls the transition of the endoderm to a pseudostratified, cell emergent epithelium for liver bud development. Dev Biol. 2006;290:44-56.

18. Fukuda A, Kawaguchi Y, Furuyama K, Kodama S, Kuhara T, Horiguchi M, Koizumi M, Fujimoto K, Doi R, Wright CV, Chiba T. Loss of the major duodenal papilla results in brown pigment biliary stone formation in pdx1 null mice. Gastroenterology. 2006;130:855-867.

19. Sumazaki R, Shiojiri N, Isoyama S, Masu M, Keino-Masu K, Osawa M, Nakauchi H, Kageyama R, Matsui A. Conversion of biliary system to pancreatic tissue in Hes1-deficient mice. Nat Genet. 2004;36:83-87.

20. Scott F. Gilbert. Developmental Biology, 9th Edition. SINAUER. 2010.

21. Knoblich JA. Mechanisms of asymmetric stem cell division. Cell. 2008;132:583-597.

22. Barker N, Bartfeld S, Clevers H. Tissue-resident adult stem cell populations of rapidly self-renewing organs. Cell Stem Cell. 2010;7:656-670.

23. Morrison SJ, Spradling AC. Stem cells and niches: mechanisms that promote stem cell maintenance throughout life. Cell. 2008;132:598-611.

24. Kretzschmar K, Watt FM. Lineage tracing. Cell. 2012;148:33-45.

25. Miyajima A, Tanaka M, Itoh T. Stem/progenitor cells in liver development, homeostasis, regeneration, and reprogramming. Cell Stem Cell. 2014;14:561-574.

26. Farber E. Similarities in the sequence of early histological changes induced in the liver of the rat by ethionine, 2-acetylamino-fluorene, and 3'-methyl-4-dimethylaminoazobenzene. Cancer Res. 1956;16:142-148.

27. Lowes KN, Brennan BA, Yeoh GC, Olynyk JK. Oval cell numbers in human chronic liver diseases are directly related to disease severity. Am. J. Pathol. 1999;154:537–541.

28. Sun C, Jin XL, Xiao JC. Oval cells in hepatitis B virus-positive and hepatitis C virus-positive liver cirrhosis: histological and ultrastructural study. Histopathology. 2006;48:546-555.

29. Spee B, Carpino G, Schotanus BA, Katoonizadeh A, Vander Borght S, Gaudio E, Roskams T. Characterisation of the liver progenitor cell niche in liver diseases: potential involvement of Wnt and Notch signalling. Gut. 2010;59:247-257.

30. Baumann U, Crosby HA, Ramani P, Kelly DA, Strain AJ. Expression of the stem cell factor receptor c-kit in normal and diseased pediatric liver: identification of a human hepatic progenitor cell? Hepatology. 1999;30:112-117.

31. Nobili V, Carpino G, Alisi A, Franchitto A, Alpini G, De Vito R, Onori P, Alvaro D, Gaudio E. Hepatic progenitor cells activation, fibrosis, and adipokines production in pediatric nonalcoholic fatty liver disease. Hepatology. 2012;56:2142-2153.

32. Richardson MM, Jonsson JR, Powell EE, Brunt EM, Neuschwander-Tetri BA, Bhathal PS, Dixon JB, Weltman MD, Tilg H, Moschen AR, Purdie DM, Demetris AJ, Clouston AD. Progressive fibrosis in nonalcoholic steatohepatitis: association with altered regeneration and a ductular reaction. Gastroenterology. 2007;133:80-90.

33. Factor VM, Radaeva SA, Thorgeirsson SS. Origin and fate of oval cells in dipin-induced hepatocarcinogenesis in the mouse. Am J Pathol. 1994;145:409-422.

34. Preisegger KH, Factor VM, Fuchsbichler A, Stumptner C, Denk H, Thorgeirsson SS. Atypical ductular proliferation and its inhibition by transforming growth factor beta1 in the 3,5-diethoxycarbonyl-1,4-dihydrocollidine mouse model for chronic alcoholic liver disease. Lab Invest. 1999;79:103-109.

35. Rosenberg D, Ilic Z, Yin L, Sell S. Proliferation of hepatic lineage cells of normal C57BL and interleukin-6 knockout mice after cocaine-induced periportal injury. Hepatology. 2000;31:948-955.

36. Lee JH, Ilic Z, Sell S. Cell kinetics of repair after allyl alcohol-induced liver necrosis in mice. Int J Exp Pathol. 1996;77:63-72.

37. Knight B, Yeoh GC, Husk KL, Ly T, Abraham LJ, Yu C, Rhim JA, Fausto N. Impaired preneoplastic changes and liver tumor formation in tumor necrosis factor receptor type 1 knockout mice. J Exp Med. 2000;192:1809-1818.

38. Akhurst B, Croager EJ, Farley-Roche CA, Ong JK, Dumble ML, Knight B, Yeoh GC. A modified choline-deficient, ethionine-supplemented diet protocol effectively induces oval cells in mouse liver. Hepatology. 2001;34:519-522.

39. Sackett SD, Li Z, Hurtt R, Gao Y, Wells RG, Brondell K, Kaestner KH, Greenbaum LE. Foxl1 is a marker of bipotential hepatic progenitor cells in mice. Hepatology. 2009;49:920-929.

40. Gleiberman AS, Encinas JM, Mignone JL, Michurina T, Rosenfeld MG, Enikolopov G. Expression of nestin-green fluorescent protein transgene marks oval cells in the adult liver. Dev Dyn. 2005;234:413-421.

41. Jung Y, Brown KD, Witek RP, Omenetti A, Yang L, Vandongen M, Milton RJ, Hines IN, Rippe RA, Spahr L, Rubbia-Brandt L, Diehl AM. Accumulation of hedgehog-responsive progenitors parallels alcoholic liver disease severity in mice and humans. Gastroenterology. 2008;134:1532-1543.

42. Endo Y, Zhang M, Yamaji S, Cang Y. Genetic abolishment of hepatocyte proliferation activates hepatic stem cells. PLoS One. 2012;7:e31846.

43. Lu WY, Bird TG, Boulter L, Tsuchiya A, Cole AM, Hay T, Guest RV, Wojtacha D, Man TY, Mackinnon A, Ridgway RA, Kendall T, Williams MJ, Jamieson T, Raven A, Hay DC, Iredale JP, Clarke AR, Sansom OJ, Forbes SJ. Hepatic progenitor cells of biliary origin with liver repopulation capacity. Nat Cell Biol. 2015;17:971-983.

44. Teebor GW, Becker FF. Regression and persistence of hyperplastic hepatic nodules induced by N-2-Fluorenylacetamide and their relationship to hepatocarcinogenesis. Cancer Res. 1971;31:1-3.

45. Schwarze PE, Pettersen EO, Shoaib MC, Seglen PO. Emergence of a population of small, diploid hepatocytes during hepatocarcinogenesis. Carcinogenesis. 1984;5:1267-1275.

46. Solt DB, Medline A, Farber E. Rapid emergence of carcinogen-induced hyperplastic lesions in a new model for the sequential analysis of liver carcinogenesis. Am J Pathol. 1977;88:595-618.

47. Evarts RP, Nagy P, Marsden E, Thorgeirsson SS. A precursor-product relationship exists between oval cells and hepatocytes in rat liver. Carcinogenesis. 1987;8:1737-1740.

48. Evarts RP, Nakatsukasa H, Marsden ER, Hsia CC, Dunsford HA, Thorgeirsson SS. Cellular and molecular changes in the early stages of chemical hepatocarcinogenesis in the rat. Cancer Res. 1990;50:3439-3444.

49. Petersen BE, Goff JP, Greenberger JS, Michalopoulos GK. Hepatic oval cells express the hematopoietic stem cell marker Thy-1 in the rat. Hepatology. 1998;27:433-445.

50. Yavorkovsky L, Lai E, Ilic Z, Sell S. Participation of small intraportal stem cells in the restitutive response of the liver to periportal necrosis induced by allyl alcohol. Hepatology. 1995;21:1702-1712.

51. Shinozuka H, Lombardi B, Sell S, Iammarino RM. Early histological and functional alterations of ethionine liver carcinogenesis in rats fed a choline-deficient diet. Cancer Res. 1978;38:1092-1098.

52. Lesch R, Reutter W, Keppler D, Decker K. Liver restitution after acute galactosamine hepatitis: autoradiographic and biochemical studies in rats. Exp Mol Pathol. 1970;12:58-

53. Lemire JM, Shiojiri N, Fausto N. Oval cell proliferation and the origin of small hepatocytes in liver injury induced by D-galactosamine. Am J Pathol. 1991;139:535-552.

54. Dabeva MD, Shafritz DA. Activation, proliferation, and differentiation of progenitor cells into hepatocytes in the D-galactosamine model of liver regeneration. Am J Pathol. 1993;143:1606-1620.

55. Laconi E, Sarma DS, Pani P. Transplantation of normal hepatocytes modulates the development of chronic liver lesions induced by a pyrrolizidine alkaloid, lasiocarpine. Carcinogenesis. 1995;16:139-142.

56. Yasui O, Miura N, Terada K, Kawarada Y, Koyama K, Sugiyama T. Isolation of oval cells from Long-Evans Cinnamon rats and their transformation into hepatocytes in vivo in the rat liver. Hepatology. 1997;25:329-334.

57. Laconi E, Oren R, Mukhopadhyay DK, Hurston E, Laconi S, Pani P, Dabeva MD, Shafritz DA. Long-term, near-total liver replacement by transplantation of isolated hepatocytes in rats treated with retrorsine. Am J Pathol. 1998;153:319-329.

58. Gordon GJ, Coleman WB, Hixson DC, Grisham JW. Liver regeneration in rats with retrorsine-induced hepatocellular injury proceeds through a novel cellular response. Am J Pathol. 2000;156:607-619.

59. Choi TY, Ninov N, Stainier DY, Shin D. Extensive conversion of hepatic biliary epithelial cells to hepatocytes after near total loss of hepatocytes in zebrafish. Gastroenterology. 2014;146:776-788.

60. Roskams T, De Vos R, Desmet V. 'Undifferentiated progenitor cells' in focal nodular hyperplasia of the liver. Histopathology. 1996;28:291-299.

61. Schmelzer E, Zhang L, Bruce A, Wauthier E, Ludlow J, Yao HL, Moss N, Melhem A, McClelland R, Turner W, Kulik M, Sherwood S, Tallheden T, Cheng N, Furth ME,

Reid LM. Human hepatic stem cells from fetal and postnatal donors. J Exp Med. 2007;204:1973-1987.

62. Crosby HA, Kelly DA, Strain AJ. Human hepatic stem-like cells isolated using c-kit or CD34 can differentiate into biliary epithelium. Gastroenterology. 2001;120:534-544.

63. Baumann U, Crosby HA, Ramani P, Kelly DA, Strain AJ. Expression of the stem cell factor receptor c-kit in normal and diseased pediatric liver: identification of a human hepatic progenitor cell? Hepatology. 1999;30:112-117.

64. Crosby HA, Hubscher SG, Joplin RE, Kelly DA, Strain AJ. Immunolocalization of OV-6, a putative progenitor cell marker in human fetal and diseased pediatric liver. Hepatology. 1998;28:980-985.

65. Dollé L, Best J, Empsen C, Mei J, Van Rossen E, Roelandt P, Snykers S, Najimi M, Al Battah F, Theise ND, Streetz K, Sokal E, Leclercq IA, Verfaillie C, Rogiers V, Geerts A, van Grunsven LA. Successful isolation of liver progenitor cells by aldehyde dehydrogenase activity in naïve mice. Hepatology. 2012;55:540-552.

66. Wang X, Foster M, Al-Dhalimy M, Lagasse E, Finegold M, Grompe M. The origin and liver repopulating capacity of murine oval cells. Proc Natl Acad Sci U S A. 2003;100 Suppl 1:11881-8.

67. Rountree CB, Barsky L, Ge S, Zhu J, Senadheera S, Crooks GM. A CD133-expressing murine liver oval cell population with bilineage potential. Stem Cells. 2007;25:2419-2429.

68. Suzuki A, Sekiya S, Onishi M, Oshima N, Kiyonari H, Nakauchi H, Taniguchi H. Flow cytometric isolation and clonal identification of self-renewing bipotent hepatic progenitor cells in adult mouse liver. Hepatology. 2008;48:1964-1978.

69. Kamiya A, Kakinuma S, Yamazaki Y, Nakauchi H. Enrichment and clonal culture of progenitor cells during mouse postnatal liver development in mice. Gastroenterology. 2009;137:1114-1126.

70. Okabe M, Tsukahara Y, Tanaka M, Suzuki K, Saito S, Kamiya Y, Tsujimura T, Nakamura K, Miyajima A. Potential hepatic stem cells reside in EpCAM+ cells of

normal and injured mouse liver. Development. 2009;136:1951-1960.

71. Qiu Q, Hernandez JC, Dean AM, Rao PH, Darlington GJ. CD24-positive cells from normal adult mouse liver are hepatocyte progenitor cells. Stem Cells Dev. 2011;20:2177-2188.

72. Dorrell C, Erker L, Schug J, Kopp JL, Canaday PS, Fox AJ, Smirnova O, Duncan AW, Finegold MJ, Sander M, Kaestner KH, Grompe M. Prospective isolation of a bipotential clonogenic liver progenitor cell in adult mice. Genes Dev. 2011;25:1193-1203.

73. Huch M, Dorrell C, Boj SF, van Es JH, Li VS, van de Wetering M, Sato T, Hamer K, Sasaki N, Finegold MJ, Haft A, Vries RG, Grompe M, Clevers H. In vitro expansion of single Lgr5+ liver stem cells induced by Wnt-driven regeneration. Nature. 2013a;494:247-250.

74. Engelhardt NV, Factor VM, Yasova AK, Poltoranina VS, Baranov VN, Lasareva MN. Common antigens of mouse oval and biliary epithelial cells. Expression on newly formed hepatocytes. Differentiation. 1990;45:29-37.

75. Furuyama K, Kawaguchi Y, Akiyama H, Horiguchi M, Kodama S, Kuhara T, Hosokawa S, Elbahrawy A, Soeda T, Koizumi M, Masui T, Kawaguchi M, Takaori K, Doi R, Nishi E, Kakinoki R, Deng JM, Behringer RR, Nakamura T, Uemoto S. Continuous cell supply from a Sox9-expressing progenitor zone in adult liver, exocrine pancreas and intestine. Nat Genet. 2011;43:34-41.

76. Dumble ML, Croager EJ, Yeoh GC, Quail EA. Generation and characterization of p53 null transformed hepatic progenitor cells: oval cells give rise to hepatocellular carcinoma. Carcinogenesis. 2002;23:435-445.

77. Petersen BE, Grossbard B, Hatch H, Pi L, Deng J, Scott EW. Mouse A6-positive hepatic oval cells also express several hematopoietic stem cell markers. Hepatology. 2003;37:632-640.

78. Español-Suñer R, Carpentier R, Van Hul N, Legry V, Achouri Y, Cordi S, Jacquemin P, Lemaigre F, Leclercq IA. Liver progenitor cells yield functional hepatocytes in

response to chronic liver injury in mice. Gastroenterology. 2012;143:1564-1575.

79. Rodrigo-Torres D, Affò S, Coll M, Morales-Ibanez O, Millán C, Blaya D, Alvarez-Guaita A, Rentero C, Lozano JJ, Maestro MA, Solar M, Arroyo V, Caballería J, van Grunsven LA, Enrich C, Ginès P, Bataller R, Sancho-Bru P. The biliary epithelium gives rise to liver progenitor cells. Hepatology. 2014;60:1367-1377.

80. Jörs S, Jeliazkova P, Ringelhan M, Thalhammer J, Dürl S, Ferrer J, Sander M, Heikenwalder M, Schmid RM, Siveke JT, Geisler F. Lineage fate of ductular reactions in liver injury and carcinogenesis. J Clin Invest. 2015;125:2445-2457.

81. Shin S, Walton G, Aoki R, Brondell K, Schug J, Fox A, Smirnova O, Dorrell C, Erker L, Chu AS, Wells RG, Grompe M, Greenbaum LE, Kaestner KH. Foxl1-Cre-marked adult hepatic progenitors have clonogenic and bilineage differentiation potential. Genes Dev. 2011;25:1185-1192.

82. Tatematsu M, Kaku T, Medline A, Farber E. Intestinal metaplasia as a common option of oval cells in relation to cholangiofibrosis in liver of rats exposed to 2-acetylaminofluorene. Lab Invest. 1985;52:354-362.

83. Paku S, Dezso K, Kopper L, Nagy P. Immunohistochemical analysis of cytokeratin 7 expression in resting and proliferating biliary structures of rat liver. Hepatology. 2005;42:863-870.

84. Yovchev MI, Grozdanov PN, Joseph B, Gupta S, Dabeva MD. Novel hepatic progenitor cell surface markers in the adult rat liver. Hepatology. 2007;45:139-149.

85. Omori N, Omori M, Evarts RP, Teramoto T, Miller MJ, Hoang TN, Thorgeirsson SS. Partial cloning of rat CD34 cDNA and expression during stem cell-dependent liver regeneration in the adult rat. Hepatology. 1997;26:720-727.

86. Yaswen P, Hayner NT, Fausto N. Isolation of oval cells by centrifugal elutriation and comparison with other cell types purified from normal and preneoplastic livers. Cancer Res. 1984;44:324-331.

87. Lemire JM, Fausto N. Multiple alpha-fetoprotein RNAs in adult rat liver: cell type-specific expression and differential regulation. Cancer Res. 1991;51:4656-464.

88. Fujio K, Evarts RP, Hu Z, Marsden ER, Thorgeirsson SS. Expression of stem cell factor and its receptor, c-kit, during liver regeneration from putative stem cells in adult rat. Lab Invest. 1994;70:511-516.

89. Jensen CH, Jauho EI, Santoni-Rugiu E, Holmskov U, Teisner B, Tygstrup N, Bisgaard HC. Transit-amplifying ductular (oval) cells and their hepatocytic progeny are characterized by a novel and distinctive expression of delta-like protein/preadipocyte factor 1/fetal antigen 1. Am J Pathol. 2004;164:1347-1359.

90. Dunsford HA, Karnasuta C, Hunt JM, Sell S. Different lineages of chemically induced hepatocellular carcinoma in rats defined by monoclonal antibodies. Cancer Res. 1989;49:4894-4900.

91. Evarts RP, Nagy P, Nakatsukasa H, Marsden E, Thorgeirsson SS. In vivo differentiation of rat liver oval cells into hepatocytes. Cancer Res. 1989;49:1541-1547.

92. Cardinale V, Wang Y, Carpino G, Cui CB, Gatto M, Rossi M, Berloco PB, Cantafora A, Wauthier E, Furth ME, Inverardi L, Dominguez-Bendala J, Ricordi C, Gerber D, Gaudio E, Alvaro D, Reid L. Multipotent stem/progenitor cells in human biliary tree give rise to hepatocytes, cholangiocytes, and pancreatic islets. Hepatology. 2011;54:2159-2172.

93. Carpino G, Cardinale V, Onori P, Franchitto A, Berloco PB, Rossi M, Wang Y, Semeraro R, Anceschi M, Brunelli R, Alvaro D, Reid LM, Gaudio E. Biliary tree stem/progenitor cells in glands of extrahepatic and intraheptic bile ducts: an anatomical in situ study yielding evidence of maturational lineages. J Anat. 2012;220:186-199.

94. Cardinale V, Wang Y, Carpino G, Mendel G, Alpini G, Gaudio E, Reid LM, Alvaro D. The biliary tree-a reservoir of multipotent stem cells. Nat Rev Gastroenterol Hepatol. 2012;9:231-240.

95. Lanzoni G, Cardinale V, Carpino G. The hepatic, biliary, and pancreatic network of stem/progenitor cell niches in humans: A new reference frame for disease and regeneration. Hepatology. 2016;64:277-286.

96. COHEN PJ. THE RENEWAL AREAS OF THE COMMON BILE DUCT

EPITHELIUM IN THE RAT. Anat Rec. 1964;150:237-241.

97. Kurumaya H, Ohta G, Nakanuma Y. Endocrine cells in the intrahepatic biliary tree in normal livers and hepatolithiasis. Arch Pathol Lab Med. 1989;113:143-147.

98. Sutton ME, op den Dries S, Koster MH, Lisman T, Gouw AS, Porte RJ. Regeneration of human extrahepatic biliary epithelium: the peribiliary glands as progenitor cell compartment. Liver Int. 2012;32:554-559.

99. Carpino G, Cardinale V, Renzi A, Hov JR, Berloco PB, Rossi M, Karlsen TH, Alvaro D, Gaudio E. Activation of biliary tree stem cells within peribiliary glands in primary sclerosing cholangitis. J Hepatol. 2015;63:1220-1228.

100. Carpino G, Puca R, Cardinale V, Renzi A, Scafetta G, Nevi L, Rossi M, Berloco PB, Ginanni Corradini S, Reid LM, Maroder M, Gaudio E, Alvaro D. Peribiliary Glands as a Niche of Extrapancreatic Precursors Yielding Insulin-Producing Cells in Experimental and Human Diabetes. Stem Cells. 2016;34:1332-1342.

101. Irie T, Asahina K, Shimizu-Saito K, Teramoto K, Arii S, Teraoka H. Hepatic progenitor cells in the mouse extrahepatic bile duct after a bile duct ligation. Stem Cells Dev. 2007;16:979-987.

102. Shivakumar P, Campbell KM, Sabla GE, Miethke A, Tiao G, McNeal MM, Ward RL, Bezerra JA. Obstruction of extrahepatic bile ducts by lymphocytes is regulated by IFN-gamma in experimental biliary atresia. J Clin Invest. 2004;114:322-329.

103. Li J, Razumilava N, Gores GJ, Walters S, Mizuochi T, Mourya R, Bessho K, Wang YH, Glaser SS, Shivakumar P, Bezerra JA. Biliary repair and carcinogenesis are mediated by IL-33-dependent cholangiocyte proliferation. J Clin Invest. 2014;124:3241-3251.

104. Nakagawa H, Suzuki N, Hirata Y, Hikiba Y, Hayakawa Y, Kinoshita H, Ihara S, Uchino K, Nishikawa Y, Ijichi H, Otsuka M, Arita J, Sakamoto Y, Hasegawa K, Kokudo N, Tateishi K, Koike K. Biliary epithelial injury-induced regenerative response by IL-33 promotes cholangiocarcinogenesis from peribiliary glands. Proc Natl Acad Sci U S A. 2017;114:E3806-E3815.

105. Lipinski M, Parks DR, Rouse RV, Herzenberg LA. Human trophoblast cell-surface antigens defined by monoclonal antibodies. Proc Natl Acad Sci U S A. 1981;78:5147-5150.

106. Fornaro M, Dell'Arciprete R, Stella M, Bucci C, Nutini M, Capri MG, Alberti S. Cloning of the gene encoding Trop-2, a cell-surface glycoprotein expressed by human carcinomas. Int J Cancer. 1995;62:610-618.

107. Linnenbach AJ, Wojcierowski J, Wu SA, Pyrc JJ, Ross AH, Dietzschold B, Speicher D, Koprowski H. Sequence investigation of the major gastrointestinal tumor-associated antigen gene family, GA733. Proc Natl Acad Sci U S A. 1989;86:27-31.

108. Linnenbach AJ, Seng BA, Wu S, Robbins S, Scollon M, Pyrc JJ, Druck T, Huebner K. Retroposition in a family of carcinoma-associated antigen genes. Mol Cell Biol. 1993;13:1507-1515.

109. Lin JC, Wu YY, Wu JY, Lin TC, Wu CT, Chang YL, Jou YS, Hong TM, Yang PC. TROP2 is epigenetically inactivated and modulates IGF-1R signalling in lung adenocarcinoma. EMBO Mol Med. 2012;4:472-485.

110. Basu A, Goldenberg DM, Stein R. The epithelial/carcinoma antigen EGP-1, recognized by monoclonal antibody RS7-3G11, is phosphorylated on serine 303. Int J Cancer. 1995;62:472-479.

111. El Sewedy T, Fornaro M, Alberti S. Cloning of the murine TROP2 gene: conservation of a PIP2-binding sequence in the cytoplasmic domain of TROP-2. Int J Cancer. 1998;75:324-330.

112. Tsukahara Y, Tanaka M, Miyajima A. TROP2 expressed in the trunk of the ureteric duct regulates branching morphogenesis during kidney development. PLoS One. 2011;6:e28607.

113. Mustata RC, Vasile G, Fernandez-Vallone V, Strollo S, Lefort A, Libert F, Monteyne D, Pérez-Morga D, Vassart G, Garcia MI. Identification of Lgr5-independent spheroid-generating progenitors of the mouse fetal intestinal epithelium. Cell Rep.

2013;5:421-432.

114. Fernandez Vallone V, Leprovots M, Strollo S, Vasile G, Lefort A, Libert F, Vassart G, Garcia MI. Trop2 marks transient gastric fetal epithelium and adult regenerating cells after epithelial damage. Development. 2016;143:1452-1463.

115. Goldstein AS, Lawson DA, Cheng D, Sun W, Garraway IP, Witte ON. Trop2 identifies a subpopulation of murine and human prostate basal cells with stem cell characteristics. Proc Natl Acad Sci U S A. 2008;105:20882-20887.

116. Nakatsukasa M, Kawasaki S, Yamasaki K, Fukuoka H, Matsuda A, Tsujikawa M, Tanioka H, Nagata-Takaoka M, Hamuro J, Kinoshita S. Tumor-associated calcium signal transducer 2 is required for the proper subcellular localization of claudin 1 and 7: implications in the pathogenesis of gelatinous drop-like corneal dystrophy. Am J Pathol. 2010;177:1344-1355.

117. Sun W, Wilhelmina Aalders T, Oosterwijk E. Identification of potential bladder progenitor cells in the trigone. Dev Biol. 2014;393:84-92.

118. Liu Q, Li H, Wang Q, Zhang Y, Wang W, Dou S, Xiao W. Increased expression of TROP2 in airway basal cells potentially contributes to airway remodeling in chronic obstructive pulmonary disease. Respir Res. 2016;17:159.

119. Ohmachi T, Tanaka F, Mimori K, Inoue H, Yanaga K, Mori M. Clinical significance of TROP2 expression in colorectal cancer. Clin Cancer Res. 2006;12:3057-3063.

120. Fong D, Spizzo G, Gostner JM, Gastl G, Moser P, Krammel C, Gerhard S, Rasse M, Laimer K. TROP2: a novel prognostic marker in squamous cell carcinoma of the oral cavity. Mod Pathol. 2008a;21:186-191.

121. Fong D, Moser P, Krammel C, Gostner JM, Margreiter R, Mitterer M, Gastl G, Spizzo G. High expression of TROP2 correlates with poor prognosis in pancreatic cancer. Br J Cancer. 2008b;99:1290-1295.

122. Mühlmann G, Spizzo G, Gostner J, Zitt M, Maier H, Moser P, Gastl G, Zitt M, Müller HM, Margreiter R, Ofner D, Fong D. TROP2 expression as prognostic marker

for gastric carcinoma. J Clin Pathol. 2009;62:152-158.

123. Lin H, Zhang H, Wang J, Lu M, Zheng F, Wang C, Tang X, Xu N, Chen R, Zhang D, Zhao P, Zhu J, Mao Y, Feng Z. A novel human Fab antibody for Trop2 inhibits breast cancer growth in vitro and in vivo. Int J Cancer. 2014;134:1239-1249.

124. Stoyanova T, Goldstein AS, Cai H, Drake JM, Huang J, Witte ON. Regulated proteolysis of Trop2 drives epithelial hyperplasia and stem cell self-renewal via β-catenin signaling. Genes Dev. 2012;26:2271-2285.

125. Cubas R, Zhang S, Li M, Chen C, Yao Q. Trop2 expression contributes to tumor pathogenesis by activating the ERK MAPK pathway. Mol Cancer. 2010;9:253.

126. Liu T, Liu Y, Bao X, Tian J, Liu Y, Yang X. Overexpression of TROP2 predicts poor prognosis of patients with cervical cancer and promotes the proliferation and invasion of cervical cancer cells by regulating ERK signaling pathway. PLoS One. 2013;8:e75864.

127. Ripani E, Sacchetti A, Corda D, Alberti S. Human Trop-2 is a tumor-associated calcium signal transducer. Int J Cancer. 1998;76:671-676.

128. Maetzel D, Denzel S, Mack B, Canis M, Went P, Benk M, Kieu C, Papior P, Baeuerle PA, Munz M, Gires O. Nuclear signalling by tumour-associated antigen EpCAM. Nat Cell Biol. 2009;11:162-171.

129. Wu CJ, Mannan P, Lu M, Udey MC. Epithelial cell adhesion molecule (EpCAM) regulates claudin dynamics and tight junctions. J Biol Chem. 2013;288:12253-12268.

130. McDougall AR, Tolcos M, Hooper SB, Cole TJ, Wallace MJ. Trop2: from development to disease. Dev Dyn. 2015;244:99-109.

131. Ke MT, Fujimoto S, Imai T. SeeDB: a simple and morphology-preserving optical clearing agent for neuronal circuit reconstruction. Nat Neurosci. 2013;16:1154-1161.

132. Tanimizu N, Nishikawa Y, Ichinohe N, Akiyama H, Mitaka T. Sry HMG box protein 9-positive (Sox9+) epithelial cell adhesion molecule-negative (EpCAM-) biphenotypic cells derived from hepatocytes are involved in mouse liver regeneration. J Biol Chem 2014;289:7589-7598.

133. Huch M, Bonfanti P, Boj SF, Sato T, Loomans CJ, van de Wetering M, Sojoodi M, Li VS, Schuijers J, Gracanin A, Ringnalda F, Begthel H, Hamer K, Mulder J, van Es JH, de Koning E, Vries RG, Heimberg H, Clevers H. Unlimited in vitro expansion of adult bi-potent pancreas progenitors through the Lgr5/R-spondin axis. EMBO J. 2013b;32:2708-2721.

134. Sampaziotis F, de Brito MC, Madrigal P, Bertero A, Saeb-Parsy K, Soares FAC, Schrumpf E, Melum E, Karlsen TH, Bradley JA, Gelson WT, Davies S, Baker A, Kaser A, Alexander GJ, Hannan NRF, Vallier L. Cholangiocytes derived from human induced pluripotent stem cells for disease modeling and drug validation. Nat Biotechnol. 2015;33:845-852.

135. Venter J, Francis H, Meng F, DeMorrow S, Kennedy L, Standeford H, Hargrove L, Wu N, Wan Y, Frampton G, McMillin M, Marzioni M, Gaudio E, Onori P, Glaser S, Alpini G. Development and functional characterization of extrahepatic cholangiocyte lines from normal rats. Dig Liver Dis. 2015;47:964-972.

136. Nakanishi Y, Seno H, Fukuoka A, Ueo T, Yamaga Y, Maruno T, Nakanishi N, Kanda K, Komekado H, Kawada M, Isomura A, Kawada K, Sakai Y, Yanagita M, Kageyama R, Kawaguchi Y, Taketo MM, Yonehara S, Chiba T. Dclk1 distinguishes between tumor and normal stem cells in the intestine. Nat Genet. 2013;45:98-103

137. Hald J, Galbo T, Rescan C, Radzikowski L, Sprinkel AE, Heimberg H, Ahnfelt-Rønne J, Jensen J, Scharfmann R, Gradwohl G, Kaestner KH, Stoeckert C Jr, Jensen JN, Madsen OD. Pancreatic islet and progenitor cell surface markers with cell sorting potential. Diabetologia. 2012;55:154-165.

138. Cogger KF, Sinha A, Sarangi F, McGaugh EC, Saunders D, Dorrell C, Mejia-Guerrero S, Aghazadeh Y, Rourke JL, Screaton RA, Grompe M, Streeter PR, Powers AC, Brissova M, Kislinger T, Nostro MC. Glycoprotein 2 is a specific cell surface marker of human pancreatic progenitors. Nat Commun. 2017;8:331.

139. van der Flier LG, Haegebarth A, Stange DE, van de Wetering M, Clevers H. OLFM4 is a robust marker for stem cells in human intestine and marks a subset of

colorectal cancer cells. Gastroenterology. 2009a;137:15-17

140. van der Flier LG, van Gijn ME, Hatzis P, Kujala P, Haegebarth A, Stange DE, Begthel H, van den Born M, Guryev V, Oving I, van Es JH, Barker N, Peters PJ, van de Wetering M, Clevers H. Transcription factor achaete scute-like 2 controls intestinal stem cell fate. Cell. 2009b;136:903-912.

141. Gigliozzi A, Fraioli F, Sundaram P, Lee J, Mennone A, Alvaro D, Boyer JL. Molecular identification and functional characterization of Mdr1a in rat cholangiocytes. Gastroenterology. 2000;119:1113-1122.

142. Sampaziotis F, Justin AW, Tysoe OC, Sawiak S, Godfrey EM, Upponi SS, Gieseck RL 3rd, de Brito MC, Berntsen NL, Gómez-Vázquez MJ, Ortmann D, Yiangou L, Ross A, Bargehr J, Bertero A, Zonneveld MCF, Pedersen MT, Pawlowski M, Valestrand L, Madrigal P, Georgakopoulos N, Pirmadjid N, Skeldon GM, Casey J, Shu W, Materek PM, Snijders KE, Brown SE, Rimland CA, Simonic I, Davies SE, Jensen KB, Zilbauer M, Gelson WTH, Alexander GJ, Sinha S, Hannan NRF, Wynn TA, Karlsen TH, Melum E, Markaki AE, Saeb-Parsy K, Vallier L. Reconstruction of the mouse extrahepatic biliary tree using primary human extrahepatic cholangiocyte organoids. Nat Med. 2017;23:954-963.

143. Trerotola M, Cantanelli P, Guerra E, Tripaldi R, Aloisi AL, Bonasera V, Lattanzio R, de Lange R, Weidle UH, Piantelli M, Alberti S. Upregulation of Trop-2 quantitatively stimulates human cancer growth. Oncogene. 2013;32:222-233.

144. Wang J, Day R, Dong Y, Weintraub SJ, Michel L. Identification of Trop-2 as an oncogene and an attractive therapeutic target in colon cancers. Mol Cancer Ther. 2008;7:280-285.

145. Tanimizu N, Nishikawa M, Saito H, Tsujimura T, Miyajima A. Isolation of hepatoblasts based on the expression of Dlk/Pref-1. J Cell Sci. 2003;116(Pt 9):1775-1786.

Acknowledgements

I would like to express a great appreciation for Prof. A. Miyajima and Associate Prof. M. Tanaka for giving me a great opportunity to carry out research and their strict mentorship.

I also thank Dr. T. Yagai, Dr. K. Kamimoto and Y. Kamiya for teaching experimental technique, N. Miyata and C. Koga for cell sorting, N. Imaizumi for animal care, Prof. K. Harada (Kanazawa University) for staining human samples, Associate Prof. N. Tanimizu (Sapporo Medical University) and H. Oyama for technical advice on cell culture, The University of Tokyo IMCB Olympus Bioimaging Center (TOBIC) for acquiring imaging data and members of the Miyajima and the Okochi laboratory for helpful discussion and comments.

Finally, I would like to thank my parents for supporting me in all aspects.